Thesis for the Degree of Doctor of Philosophy

Circumventing Spectrum Mismatch

Studies of Triplet-Triplet Annihilation Upconversion, Singlet Fission and Two-Photon Absorption in Photoactive Materials

DEISE FERNANDA BARBOSA DE MATTOS

Department of Chemistry and Chemical Engineering

CHALMERS UNIVERSITY OF TECHNOLOGY

Gothenburg, Sweden 2023

Circumventing Spectrum Mismatch
Studies of Triplet-Triplet Annihilation Upconversion, Singlet Fission and Two-Photon Absorption in Photoactive Materials

DEISE FERNANDA BARBOSA DE MATTOS

ISBN: 978-91-7905-939-2

Dorktorsavhandlingar vid Chalmers Tekniska Högskola

Ny serie nr: 5405

ISSN: 0346-718X

Department of Chemistry and Chemical Engineering

Chalmers University of Technology

SE-412 96 Gothenburg

Telephone +46 (0)31-772 1000

Cover: Schematic illustration of triplet-triplet annihilation upconversion, singlet fission and two-photon absorption in the photoactive materials studied in this work.

Printed by Chalmers Digitaltryck

Gothenburg, Sweden 2023

Circumventing Spectrum Mismatch
Studies of Triplet-Triplet Annihilation Upconversion, Singlet Fission and Two-Photon Absorption in Photoactive Materials

Deise Fernanda Barbosa de Mattos

Department of Chemistry and Chemical Engineering
Chalmers University of Technology

ABSTRACT

Solar energy stands out for its potential to supply the global energy demand by itself. Therefore, it is of great value to expand the use of processes that involve light such as conversion to electricity or fuels, or to drive high-energy reactions. However, the limited availability of photons with the desired energy required to induce a certain photophysical process poses a challenge. To circumvent this spectral mismatch, processes that up- and down-convert photon energy can be used. In this work the focus lies on photon upconversion through triplet-triplet annihilation (TTA-UC) and two-photon absorption (2PA) and downconversion through singlet fission (SF).

One key challenge for up- and downconversion processes is that for them to be useful they must be incorporated into practical devices. Therefore, one of the overall objectives of this work is to evaluate photoactive materials that both change the photon energy and have potential to be incorporated with a working device. This means moving away from diffusion control in liquid solution.

Self-assembling organogels, with chromophores covalently attached to the gelator backbone, were tested as platforms for TTA-UC and SF. The results show that chromophore-chromophore interactions can be tuned by choice of substitution position, and that it is possible to obtain photon energy conversion in the studied self-assembling gels, although efficiencies need to be improved for practical applications. The results indicate that there is potential for future development of gel-based self-assembled photoactive materials.

To demonstrate how TTA-UC can be applied to circumvent spectral mismatches in devices, it was used to sensitize the well-known catalyst titanium dioxide (TiO_2). A TTA-UC solution was used to absorb visible light and the upconverted emission was in turn used to sensitize a TiO_2 thin film. Despite needs for optimizing the setup, visible light photoexcitation could be confirmed and the number of holes in valence band could be quantified to μM concentrations, using a redox couple, which at the same time confirmed the reactivity of the sensitized TiO_2.

Keywords: triplet-triplet annihilation upconversion, singlet fission, two-photon absorption, photochemistry, energy transfer, self-assembly gels, carbon nitride quantum dots, solar energy conversion, spectroscopy.

LIST OF PUBLICATIONS

This thesis is based on the work contained in the following papers:

I. Covalent incorporation of diphenylanthracene in oxotriphenylhexanoate organogels as a quasi-solid photon upconversion matrix
Deise F. Barbosa de Mattos, Ambra Dreos, Mark D. Johnstone, August Runemark, Claire Sauvée, Victor Gray, Kasper Moth-Poulsen, Henrik Sundén, Maria Abrahamsson
Journal of Chemical Physics 153, 214705 (2020)

II. Structure-Property Relationships in Self-Assembled TIPS-Pentacene Organogels
Mark D. Johnstone, Deise F. Barbosa de Mattos, Rasmus Ringström, Andrea Ruiu, Letizia Mencaroni, Bo Albinsson, Jerker Mårtensson, Maria Abrahamsson, Henrik Sundén
Manuscript

The supporting information printed here does not include the detailed synthetic procedure.

III. Towards TiO_2 Photochemistry with Visible-to-UV Triplet-Triplet Annihilation Upconversion
Deise F. Barbosa de Mattos, Maria Abrahamsson
Manuscript

IV. Two-Photon Absorption Characteristics of EDTA Functionalised CNQDs in Water
Liam Mistry, Deise F. Barbosa de Mattos, Hanna Larsson, Carlos Benitez Martin, Maria Abrahamsson
Manuscript

PUBLICATIONS NOT INCLUDED IN THE THESIS

- Excited State Dynamics of Bistridentate and Trisbidentate Ru^{II} Complexes of Quinoline-Pyrazole Ligands
  Lisa Fredin, Joachim Hedberg Wallenstein, Elin Sundin, Martin Jarenmark, Deise Barbosa de Mattos, Petter Persson, Maria Abrahamsson
  Inorganic Chemistry **2019** *58* (24), 16354-16363

CONTRIBUTION REPORT

Description of my contribution to the appended papers:

I. Planned and performed the photophysical experiments together with A. D. Contributed to the analysis of the data and the conclusions. Synthesis was done by M. D. J. Wrote the manuscript together with M. A.

II. Planned and performed the spectroscopy and photophysical measurements together with R.R. and M. D. J. Contributed to the analysis of the data and the conclusions. All synthesis related work was done by M. D. J. and A. R. Wrote part of the manuscript together with M. D. J, M. A., and H. S.

III. Designed and performed spectroscopic experiments and analyzed the data. Wrote the manuscript.

IV. Planned and performed the two-photon absorption experiments together with L. M and C. B. M. Contributed to the analysis of the data and the conclusions. Synthesized the quantum dots together with L. M. Proofread the paper.

LIST OF ABREVIATIONS

1PA	One Photon Absorption
2PA	Two-Photon Absorption
3D	Three Dimensional
4CzBN	2,3,5,6-tetra(9H-carbazol-9-yl)benzonitrile
A	Acceptor or Annihilator
AO	Atomic Orbitals
CB	Conduction Band
CCD	Charge-Coupled Device
CNQDs	Carbon Nitride Quantum Dots
CO_2	Carbon Dioxide
CSD	Cambridge Structural Database
D	Donor
DMSO	Dimethyl sulfoxide
DPA	9,10-Diphenylanthracene
EDTA	Ethylenediaminetetraacetic Acid
ESA	Excited State Absorption
ET	Electron Transfer
GSB	Ground State Bleach
HOMO	Highest Occupied Molecular Orbital
I_2/I^-	Iodine/Iodide
I_3^-	Triiodide Ion
IC	Internal Conversion
IR	Infrared Light
IRF	Instrument Response Function
ISC	Intersystem Crossing
LED	Light Emitting Diode
LiI	Lithium Iodide
LUMO	Lowest Unoccupied Molecular Orbital
MeCN	Acetonitrile
NIR	Near Infrared
OTHO	Oxotriphenylhexanoate
PdTPP	Palladium tetraphenylporphyrin
PMT	Photomultiplier Tube
PPO	2,5-Diphenyloxazole
PtOEP	Platinum Octaethylporphyrin
QDs	Quantum Dots
S	Sensitizer
S_0	Ground State
S_1	First Singlet State
S_2	Second Singlet State
SF	Singlet Fission
s-TTA	Sensitizer Triplet-Triplet Annihilation
T_1	First Triplet State

TCSPC	Time-Correlated Single-Photon Counting
TET	Triplet Energy Transfer
TIO_2	Titanium Dioxide
TIPS-PC	6,13-Bis(triisopropylsilylethynyl)pentacene
TT	Correlated Triplet Pair
TTA	Triplet-Triplet Annihilation
UC	Upconversion
UV	Ultraviolet Light
VB	Valence Band
Vis	Visible Light
VR	Vibrational Relaxation
WO_3	Tungsten Oxide

TABLE OF CONTENTS

1 INTRODUCTION

Light plays an important role in the development of human life on Earth. Without it there would be neither oxygen nor food, which come from photosynthesis.[1] Understanding the nature of light, how to control its properties and apply it to our needs has been a subject of investigation since it was possible to control fire for use as lighting. Today, the behavior of light and its interactions with matter are described by quantum theory,[2] and the applications extend to countless areas, such as photovoltaics[3, 4], photochemistry[5, 6], phototherapy[7, 8], and many everyday applications.

Given the environmental scenario in which it is necessary to limit global warming, many countries have in their action plan to increase the conversion of solar energy. In addition to use sunlight for heating and electricity, it would be beneficial to increase the use of light to assist chemical reactions[9-12] and produce fuels.[13-16] To expand the use of light it is still necessary to overcome the limited availability of photons with sufficient energy to meet the requirements of a given application. For example, there is little availability of sunlight for processes that require high-energy photons in the ultraviolet (UV) range, as only 5% of the solar spectrum that reaches the Earth's surface[17] (Fig. 1.1) has this composition.

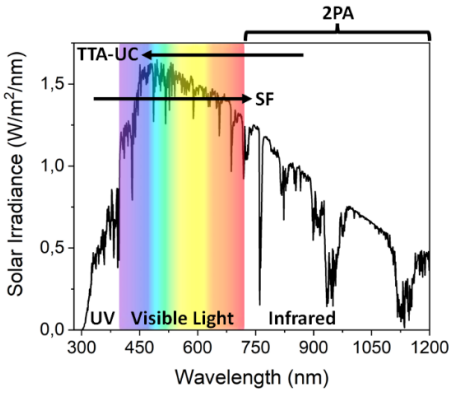

Figure 1.1. Solar irradiance spectrum on the Earth´s surface and the classification of the electromagnetic spectrum in UV (100 to 400 nm), visible light (400 to 700 nm) and infrared (above 700 nm) in relation to the wavelength. The photon up- and downconversion processes discussed in this work are indicated in the figure.

Single junction solar cells, such as silicon, have an efficiency limit of around 32%.[18] This is due to the fact that photons with energy below the bandgap have no effect, as they cannot be absorbed, and higher energy photons are absorbed and lose their excess energy through thermalization. To efficiently incorporate photons that mismatch the bandgap, up- and downconversion processes can be used.[4, 19, 20]

The downconversion process can be achieved by a mechanism called singlet fission (SF).[4, 20, 21] In this, one high-energy photon is absorbed by a chromophore and is converted into two triplet excited states that can be injected directly into a

semiconductor. For silicon solar cell the bandgap is 1.1 eV (~ 1100 nm) and SF could downconvert the visible photons, to be incorporated by the cell.[4]

Upconversion (UC) can be achieved through a number of processes including but not limited to two-photon absorption (2PA), and triplet-triplet annihilation (TTA). The use of each process depends on the available excitation light.[22-24] In TTA-UC two low energy photons are absorbed and fused into one high energy photon that is emitted by the sytem.[19] TTA-UC can be performed with low excitation power density and non-coherent light. This can be beneficial for many areas of applications such as solar cells,[4, 25-27] hydrogen production,[13, 17, 28-30] 3D printing,[31, 32] photocatalysis,[19, 33-35] and bioimaging[33, 36, 37]. In the case of 2PAa molecule or material absorbs two long-wavelength photons.[38] This requires the use of coherent light and high excitation power density, such as an ultrafast pulsed laser. 2PA has gained a lot of interest in the study of biological tissue due to the longer penetration depth of infrared photons compared to photons in the UV and visible regions, which are often a single photon absorption process.[38-43]

Although SF, TTA-UC and 2PA are promising to increase the efficiency of photoinduced processes in several areas, it is still necessary to better understand their photophysical mechanisms and how to efficiently incorporate them into practical devices. In this context, the studies that are part of this thesis are based on two objectives. First, to evaluate different photoactive materials as a platform for TTA-UC, SF and 2PA. Second, to show how Vis-to-UV TTA-UC can be used to circumvent spectral mismatches for a semiconductor.

In this thesis, easily synthesized self-assembly systems, formed by chromophores covalently bound to a low molecular weight gelator, were photophysically characterized and tested as a platform for TTA-UC and SF. It is hypothesized that it is possible to control the orientation of chromophores, and to facilitate the desired energy transfer processes between them.

Another study presented here explores the use of the fluorescence emission of TTA-UC, from Vis-to-UV in solution, to photoexcite titanium dioxide (TiO_2 – a known catalyst), whose bandgap is around 3.4 eV, an energy equivalent to 365 nm. The hypothesis is that it is possible to perform reactions with TiO_2 films using visible photons through Vis-to-UV TTA-UC.

In this work, we also investigated the near infrared (NIR) 2PA properties of carbon nitride quantum dots (CNQDs). These water-soluble and non-toxic CNQDs have been utilized as sensitizers in CO_2 reduction schemes with one poton-absorption[44] and may be suitable for multi-photon microscopy of biological tissues.

2 THEORY

This chapter briefly describes how interactions between light and matter occur. It also contains an overview of the photophysical and photochemical processes relevant for the work presented in this thesis.

2.1 Light-Matter Interactions

Light is radiation that has both wave and particle character. The wave is described as an oscillating electromagnetic field divided into two perpendicular components, an electric and a magnetic field. The particles are called photons and have a discrete energy, E, which is related to the wavelength (λ) or the frequency (ν) of the electromagnetic wave, the speed of light (c) and Planck´s constant through Equation 2.1.[2]

$$E = h\nu = \frac{hc}{\lambda} \tag{2.1}$$

Electrons are negatively charged particles that move around a nucleus containing positive and neutral particles. These particles form atoms, which, through chemical bonds, build up molecules and materials. Solutions of the Schrödinger equation, for the wavefunctions of the electrons that form the atoms, result in the probability of finding electrons in a given space location which are called atomic orbitals (AO). They have discrete energy levels and, according to the Aufbau principle, the electronic configuration is made from the lowest to the highest AO in energy. If there are AO with the same energy, Hund´s rule states that first they are singly occupied by electrons in the same spin (unpaired). Then, other electrons can occupy these orbitals following Pauli Exclusion Principle, where each orbital is occupied by at most two electrons with opposite spin (paired electrons). In a molecule, the linear combination of AO results in the molecular orbitals. The same rules of the AO are applied for electronic distribution in the molecular orbitals. The highest energy occupied molecular orbital is called HOMO (highest occupied molecular orbital) and the first empty orbital LUMO (lowest unoccupied molecular orbital). The possible orientations of the electron spin in a molecule are described by the multiplicity. If all electrons are paired, the molecule is said to be in a singlet state multiplicity. If two electrons are unpaired the molecule is in a triplet state multiplicity.[2, 45, 46]

In semiconductors the electrons are distributed in continuous energy bands where they are not associated to a certain orbital. The highest energy band occupied by electrons is called the valence band and the lowest vacant one is called the conduction band. The energy difference between them is the bandgap.[47, 48] Semiconductors can have their dimensions reduced to nanometer scale and the properties begin to present themselves as quantum features, the so called "artificial atoms". Therefore, as a smaller number of atoms are present in the nanocrystal than in the bulk material, the energy levels become discrete. Quantum dots (QDs) are semiconductor nanocrystals with a size between 1.5 and 10 nm, whose optical and electronic properties vary according to the size of the particle. This occurs because the bandgap energy changes, resultant of the quantum confinement effects. This is to say that, due to the

small size of the material, it is more difficult to separate the electron-hole pair formed by photoexcitation. Therefore, different sizes result in different bandgaps, which allows for tuning of the absorption range and the photoluminescence according to the application.[49-51] The work present in this thesis includes studies on molecules, quantum dots and materials such semiconductors.

When radiation impinges on matter it can be transmitted, if there is no interaction, it can be scattered, or it can be absorbed if the energy corresponds to the difference of two energy levels. Depending on the photon energy, the absorption of a photon can lead to rotational, vibrational or electronic excitation.[46, 52] The work presented here mainly deals with electronic transitions.

2.2 Photon Absorption Processes

Electronic transitions occur when UV-Vis light is absorbed by matter. Franck-Condon´s Principle states that only electrons participate in the transition between orbitals because they have lighter mass than the nuclei and absorption rate is around 10^{-15} s, fast enough for the nuclei to maintain their coordinates.[2, 38]

The minimum excitation energy for molecules is the energy difference between HOMO and LUMO. A single photon, whose energy is equal to difference between orbitals, transfer its energy ($h\nu$) to an electron which is promoted from the HOMO ($E_{initial}$) to an orbital with a higher energy level (E_{final}), Equation 2.2. The same is valid for semiconductors, if the incoming photon has energy that matches the bandgap, an electron is excited and moves to the conduction band leaving behind a hole in the valence band.[52]

$$\Delta E = E_{final} - E_{initial} = h\nu \tag{2.2}$$

The transition of the electron is considered allowed if the multiplicity of the final state is the same as the initial. Furthermore, the wavefunctions of the initial ($\Psi_{initial}$) and final (Ψ_{final}) states should overlap, and the better they are coupled the higher the probability the transition occurs. This probability is given by the Fermi Golden Rule (Eq. 2.3).[45, 53]

$$k = \frac{2\pi}{\hbar}\rho\,\langle \Psi_{initial}|H|\,\Psi_{final}\rangle^2 \tag{2.3}$$

where k is the rate at which the transition happens, $\hbar$ is the Plank constant divided by 2π, ρ is the density of states, H is the Hamiltonian, which is the operator for the absorption process when the molecule is perturbed by the oscillating electric field of the electromagnetic radiation, whose interaction with the electrons induces a transition dipole moment in the molecule due to the redistribution of charge.

Instead of one single photon absorption (1PA) to excite the molecule, it is under high intensity and coherent laser light possible to simultaneously absorb two photons (2PA) of the same or different wavelengths to reach the same excited state as with 1PA. This type of absorption is usually obtained with long wavelengths, as the addition of two low energy photons becomes equivalent to the energy delivered by only one photon of higher energy (Fig. 2.1-a). The mechanism used to describe 2PA considers

sequential absorption of the two photons and a temporary virtual state, causing the photons to be practically simultaneously absorbed.[38, 54]

In 1PA process, a transition is allowed when the oscillating electric field of light induces a transition dipole moment in the molecule due to the redistribution of charge. This is related to the symmetry of the molecule. For molecules that have an inversion center, the transition is allowed when the initial and final states have different symmetries, for example, the initial state is symmetric with respect to the inversion center and the final one is anti-symmetric.[2, 52] In 2PA process for molecules with an inversion center, the transitions with the same symmetry for the initial and final states are allowed as long as the virtual state has opposite symmetry to them.[54, 55]

Another difference between the absorption process, is that in 1PA the emission intensity is linearly proportional to the intensity of the light used as excitation source, while in 2PA the emission is quadratically dependent on the intensity of the light used as the excitation source, as this is a non-linear process.[38] Furthermore, to ensure the delivery of a large number of photons and increase the probability of the sample to absorb two photons simultaneously, high power for the excitation is typically required in 2PA, such as a pulsed laser with a pulse-width on the order of 10^{-12} to 10^{-15} s with peak power on the order of MW to GW.

2.3 Steady State and Time-Resolved Emission

In both 1PA and 2PA processes the molecule remains excited for a certain time until it returns through emission of a photon or non-radiative relaxation to the initial state, also called the ground state. There are many processes that can occur following excitation as illustrated in the Jablonski Diagram in Figure 2.1-a.

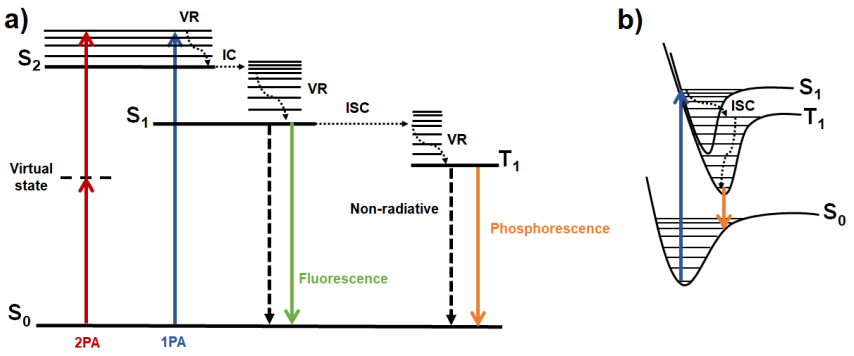

Figure 2.1. (a) Electronic transitions illustrated in a Jablonski diagram showing one (1PA) and two-photon absorption (2PA) processes, and the possible decay paths following absorption. Solid horizontal lines represent energy levels, thinner lines are vibrational levels, and thicker lines are electronic states. Vertical lines represent transitions between states. **(b)** Illustration of intersystem crossing due to the overlap between the excited singlet and triplet states.

According to Kasha´s rule, photon emission occurs from the lowest singlet or triplet state, and it is independent of the excitation wavelength. When high vibrational levels are populated the electron rapidly (10^{-12} s) releases energy by vibrational relaxation (*VR*) until it reaches the lowest level of the electronic state. From there it is possible for the electron to return to the ground state (S_0) emitting a photon or by non-radiative decay (called internal conversion, *IC*, when it occurs between states of the same multiplicity). The emitted photon has the same or lower energy than the absorbed photon. Excess energy is dissipated to arrive at the lowest energy level from which the photon is emitted. As a result, in a spectrum the emission has longer wavelengths than the absorption. This is known as Stokes shift.[38]

When light is absorbed, it does not change the spin of the electron and transitions between states of different multiplicity are forbidden. However, if there is an overlap between the potential energy curves of the singlet excited state (S_1) and the triplet state (T_1) the electron can undergo intersystem crossing, *ISC* (Fig. 2.1-b). This can be enhanced when heavy atoms, such as transition metals, are part of the molecule due to favorable spin-orbit coupling. Photon emission with no multiplicity change is called fluorescence (from S_1 to S_0), and with a spin multiplicity change is called phosphorescence (from T_1 to S_0). Usually, the spectrum and lifetime of emission for 2PA are equivalent to 1PA since the same excited state is reached.[38]

To assess how effective radiative decay is in relation to non-radiative decay the emission quantum yield (Φ) is an important parameter. It is the ratio of emitted photons to the number of absorbed photons. It is a common practice to measure Φ relative to a well characterized fluorescent substance whose Φ is known (Eq. 2.4). The reference and test sample should be measured in the same conditions.[56]

$$\Phi = \Phi_{ref} \frac{I}{I_{ref}} \frac{Abs_{ref}}{Abs} \left(\frac{\eta}{\eta_{ref}}\right)^2 \tag{2.4}$$

where the subscript ref is related to the reference substance, I is the integrated area of the emission spectrum, Abs is the absorbance at the excitation wavelength, and η is the refractive index.

Usually, fluorescence occurs on a time scale from 10^{-12} to 10^{-9} s and phosphorescence lifetime is on the order of 10^{-6} to 10 s. This difference is due to the change in the spin direction of the electron during *ISC*, which in phosphorescence reverts to the original spin direction to return to the S_0. The mathematical model of lifetime is usually exponential. When decay occurs through more than one path, a multi-exponential behavior is used as a model (Eq. 2.5). Judging whether the decay is mono- or multi-exponential is done by visualizing the proper representation of the experimental data by the model and the residuals.[38]

$$I(t) = \sum A_i exp\left(-\frac{t}{\tau_i}\right) \tag{2.5}$$

where $I(t)$ is the emission intensity, A_i is the amplitude, that is, the participation of each decay path with its respective lifetime τ_i.

If the decay is biexponential, an average lifetime can be calculated according to Equation 2.6.[25, 38, 57]

$$< \tau >= \frac{A_1 \tau_1 + A_2 \tau_2}{A_1 + A_2} \quad (2.6)$$

2.4 Photo-Induced Electron and Energy Transfer

In a photoinduced energy and electron transfer the terminology donor (D) and acceptor (A) is often used. A molecule in an excited state (D*) can interact with another molecule (A), either in its ground or excited state, transferring electrons or energy (Figure 2.2). At the end of an energy transfer there will be an excited acceptor (A*) and for electron transfer there will be charge separation, because the excited donor will have an electron removed (D^+) and the acceptor will receive the electron (A^-).[58]

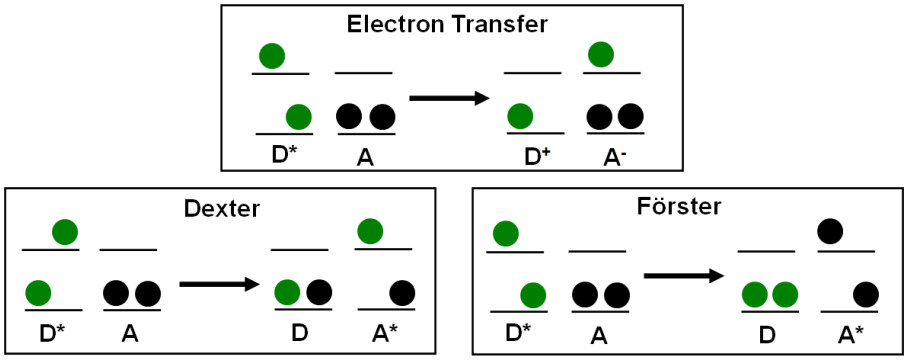

Figure 2.2. Schematic illustration of electron and energy transfer. Electron transfer results in charge separation (D^+ and A^-) while energy transfer results in an excited acceptor moiety. Note that Dexter and Förster mechanisms for energy transfer are different.

Both energy and electron transfer can often be indirectly monitored by analyzing the emission intensity and the lifetime of the excited donor. When there is a decrease in these two properties it is said that dynamic quenching has occurred, that is, when the acceptor collides with the donor and steals the excitation energy. When quenching does not depend on molecular diffusion, *e.g.* the acceptor is linked to the donor, or they may have formed a complex, and only a decrease in the emission intensity is observed (the lifetime remains constant), it is said that a static quenching occurs.[38] Distinguishing between electron and energy transfer depends on a variety of factors. For example, it may require the analysis of data obtained through the dynamics of the excited state, by transient absorption; the presence of oxidized/reduced species, by spectro-electrochemical method; and kinetics, dependent on the distance between the donor and acceptor and the polarity of the solvent.[59, 60]

2.4.1 Photo-induced Energy Transfer

We usually distinguish between two types of energy transfer, Förster and Dexter. The Förster energy transfer occurs when there is interaction between the oscillating dipole of the excited donor and the dipole of the acceptor. A Dexter-type energy transfer occurs due to overlapping molecular orbitals and there is a double exchange of electrons between the donor and acceptor. The difference between Förster and Dexter is that the former can occur when the molecules are relatively far from each other.[38, 58, 61] In the studies presented in this thesis, energy transfer occurs mainly via the Dexter mechanism. Both TTA-UC and SF are examples of energy transfer processes.

2.4.1.1 Triplet-Triplet Annihilation Upconversion

As mentioned earlier, radiative emission has lower energy than absorption (Stokes shift).[38] However, energy transfer steps can be combined to result in photon upconversion. In doing so, it is possible to obtain an anti-Stokes shift for emission which allows the circumventing of spectral mismatch in photophysical processes that require high-energy photons by absorbing low-energy ones.[19] Triplet-triplet annihilation upconversion (TTA-UC) consists of several steps of energy transfer by the Dexter mechanism, represented in Figure 2.3. A sensitizer (S) and an annihilator (A) are required. The sensitizer absorbs a low-energy photon and becomes an excited singlet. Quickly its triplet state is populated through the *ISC*. When triplet excited S encounters a ground state A, the energy is transferred to the triplet state of the annihilator, known as triplet energy transfer (TET). Two excited annihilators in proximity combine the triplet energy, also called triplet-triplet annihilation (TTA), resulting in one annihilator being promoted to the singlet state and the other returning non-radiatively to the ground state. The singlet excited annihilator emits a photon with higher energy than the photons absorbed by the sensitizers.[4, 22, 62]

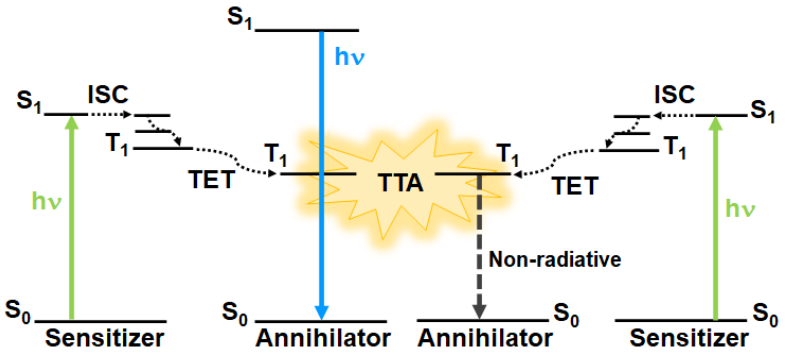

Figure 2.3. Illustration of energy transfer process required for triplet-triplet annihilation upconversion.

For a molecule to be used as a sensitizer in TTA-UC, it is desirable to have a large molar absorptivity at the excitation wavelength. The *ISC* should be efficient and the triplet state long-lived for molecular encounter with the annihilator to transfer energy. It is desirable that there is a small energy difference between the initially populated

singlet and triplet states to minimize energetic losses. In addition, the absorption of S should not overlap with the emission of the A to minimize re-absorption of the upconverted emission (the so-called secondary inner filter effect).[19]

For the annihilator, it is important that the fluorescence quantum yield is high, close to unity. The triplet state should also be long-lived and its energy lower than the triplet of the S, but with minimal difference between them to reduce energy losses. The energy of the first singlet state must be less than or equal to twice the energy of the first triplet state ($E_{S1} \leq 2 \times E_{T1}$). This last requirement is associated with combinations of spin multiplicity resulting from the fusion of the two triplets, which can be a singlet, triplet or quintet. Normally, the quintet state is energetically inaccessible. The second triplet may be accessible, but only the first singlet may result in upconverted emission.[19, 63]

The energy in the triplet state of the sensitizer can be deactivated through phosphorescence, non-radiative decay or energy transfer to the annihilator. The triplet energy in the annihilator can decay non-radiatively or be combined in the TTA. There is a minimum excitation intensity capable of making the TTA the main path and this is known as the intensity threshold (I_{th}). At excitation intensities lower than I_{th} there is a low population of triplets causing the upconversion intensity to be quadratically dependent on the excitation intensity. For intensities above I_{th} there is high formation of triplets resulting in a linear dependence on the excitation intensity. In a log-log plot of UC intensity *versus* excitation power density, I_{th} is the intersection point where the emission passes from the quadratic (slope 2) to the linear (slope 1) regime.[19, 62, 64-66]

The efficiency of the upconverted emission is evaluated according to the quantum yield. As TTA-UC works with the combination of two low energy absorbed photons for the emission of one high energy photon, the maximum quantum yield, Φ, that can be obtained is 50%. The Φ_{UC} is the product of the quantum yield of each energy transfer step (Eq. 2.7) and a spin factor (f) that considers the probability of forming an excited singlet state from TTA.[19, 64, 66, 67]

$$\Phi_{UC} = f \times \Phi_{ISC} \times \Phi_{TET} \times \Phi_{TTA} \times \Phi_f \quad (2.7)$$

where Φ_{ISC} is the intersystem crossing in the sensitizer, Φ_{TET} is the triplet energy transfer between sensitizer and annihilator, Φ_{TTA} is the triplet-triplet annihilation step and Φ_f is the fluorescence quantum yield of the annihilator.

For practical purposes, the Φ_{UC} is usually determined as described in Eq. 2.4 using a reference substance with known fluorescence quantum yield. In this case, the measured Φ_{UC} is the ratio of observed upconverted photons by the absorbed photons. It is worth noting that the quantum yield of generated photons has a greater value than the observed, because the efficiency of TTA-UC depends on the system´s environment and energy loss channels, e.g., inner filter effects, scattering.[64, 66, 67]

2.4.1.2 Singlet Fission

Another mechanism to circumvent spectral mismatch is singlet fission (SF). This is used to downconvert one high energy photon into two lower energy triplet states. The

steps of energy transfer are represented in Figure 2.4. A chromophore absorbs a photon of high energy, and it is excited to the singlet state, S_1. Another chromophore in its ground state, S_0, is in proximity and the position of these two molecules is favorable for the electronic coupling of the triplet states. Then the first chromophore shares the excitation energy with the second, thus forming a correlated triplet pair, (TT), which are coupled as an overall singlet multiplicity. This coupled triplet state is maintained until electronic coherence is lost. After that, two triplet states (T_1 + T_1) are formed and are, ideally, free to diffuse individually.[20, 68-70]

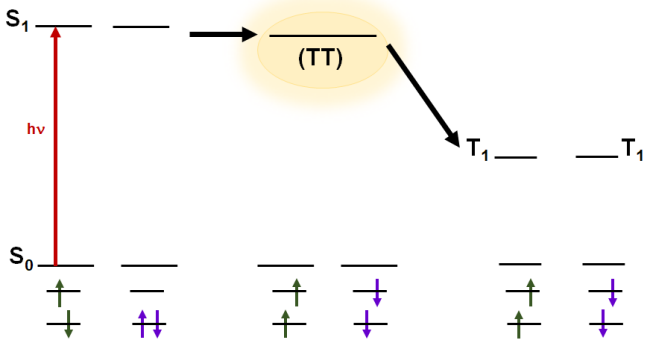

Figure 2.4. Illustration of the necessary steps for singlet fission. Below the arrows indicate the spin of each state.

For a chromophore to be used in SF it is necessary that the energy of the first singlet excited state is higher than twice the energy of the triplet state ($E_{S1} > 2\times E_{T1}$), characterizing an exergonic process. In addition, the energy of the second triplet state (E_{T2}) must be high to be inaccessible through TTA. At least a magnitude of $2\times E_{T1} < E_{T2}$ is required. Usually, the chromophore does not contain a heavy atom and the *ISC* is slow (~ 100 ns) compared to the formation of triplets from SF (~ 10 ps). The latter is faster because it is a spin allowed process, as in the formation of (*TT*) the general singlet character is conserved. The most important requirement for efficient SF is the orientation between the chromophores.[20, 69-72]

The efficiency of SF is also measured according to the quantum yield. In this case, an absorbed photon is split into two excited triplets and the maximum Φ is 200%. Usually, it is not trivial to determine SF quantum yields.

2.4.2 Photo-Induced Electron Transfer

As stated earlier and illustrated in Figure 2.2, electron transfer (ET) between a photoexcited donor (D*) and an acceptor (A) results in oxidized (D^+) and reduced species (A^-).[58] It can occur between molecules or intramolecularly, where D and A are covalently connected by a bridge or between molecules and materials such as semiconductors or quantum dots.[73-75]

In a spontaneous reaction in which the potential energy of the reactant is higher than that of the product, the Gibbs free energy (ΔG^0) is the driving force. For typical ET this is also applicable. The rate of electron transfer (k_{ET}) is described by Marcus theory (Eq. 2.8), and it is a function of ΔG^0 and the reorganization energy of the solvent (λ), which is the energy that would be needed to adjust the vibrational mode of D and A and move the electron without rearranging the solvation environment.[58, 73]

$$k_{ET} = k_{el}\, \nu_n exp\left(\frac{-\Delta G^{\neq}}{k_B T}\right) \qquad (2.8)$$

$$\Delta G^{\neq} = \frac{(\Delta G^0 + \lambda)^2}{4\lambda}$$

where k_{el} is the electronic transmission coefficient, ν_n is the nuclear frequency, $\Delta G^{\neq}$ is the free energy of activation, k_B is the Boltzmann´s constant, T is the temperature.

The diagrams of the potential energy surface are illustrated in Figure 2.5. Excitation of the donor (D* + A) changes the energy difference between D* and A and subsequently increases the driving force. Consequently, the electron transfer rate increases. This makes oxidation (or reduction) reactions easier to occur in the excited state than in the ground state.[73, 74, 76] Starting from a case where the $-\Delta G^0 < \lambda$, electron transfer occurs in the normal region. Increasing $-\Delta G^0$ to be equal to λ enhances k_{ET}, as $\Delta G^{\neq} = 0$ there is no energy barrier to reach the charge separated state ($D^+ + A^-$). In this situation the electron transfer rate is at the maximum value. If $-\Delta G^0$ is increased again, to values higher than λ, k_{ET} decreases because $\Delta G^{\neq}$ reappears. This is the so called inverted region, where k_{ET} decreases with increasing the driving force.[77]

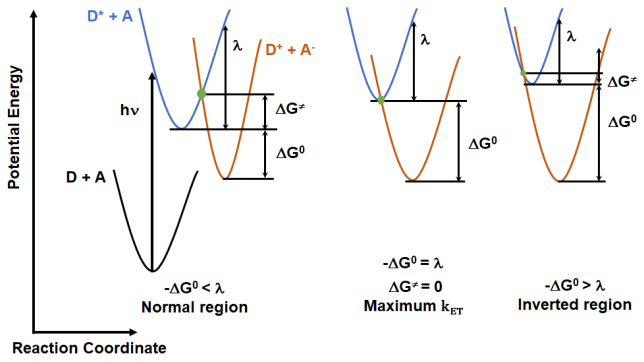

Figure 2.5. Illustration of the potential energy surface diagram in the Marcus theory. The photoinduced electron transfer occurs in the normal region. The diagram contains the ground state (D + A), the initially photoexcited state (D* + A), the charge separated state ($D^+ + A^-$).

2.4.2.1 Interfacial Electron Transfer

Instead of using a donor and an acceptor in molecular form, it is possible to perform electron transfer on surfaces of semiconductors, from a molecular species to the semiconductor and *vice versa*. One of the most well-known examples of the former is the dye sensitized solar cell where the electron injection from the dye to the

semiconductor is a good example of interfacial electron transfer. Some reactions require the transfer of more than one electron, and this can be difficult among molecules to be oxidized more than once unless a very high concentration of D would be necessary. This can be facilitated by a photoexcited semiconductor that serves as an electron reservoir.[48, 78]

Photoexcitation of the semiconductor with energy equal to or greater than the bandgap causes electrons (e^-) to be promoted from the valence band (VB) to the conduction band (CB). Holes (h^+) are left in the VB. Both the e^- and the h^+ are charge carriers that move randomly, and they can be trapped in the bulk sites, or they can migrate to the surface of the semiconductor where they also become trapped. Both in the bulk and on the surface e^- and h^+ can recombine, and the electron returns to the VB.

On the surface of the semiconductor, electrons can be accumulated and transferred to an acceptor which will be reduced, in the environment or adhered to the surface. On the other hand, a donor is oxidized by transferring electrons to the holes on the surface. Figure 2.6 illustrates the steps from photoexcitation to electron transfer on the surface of a semiconductor. For ET to occur from the semiconductor to an acceptor, it is necessary that the CB has energy greater than the energy of the acceptor orbital that will receive the electron. The opposite is true for oxidation reactions, in which the electron that will be transferred by the donor has a higher energy than the VB of the semiconductor. The reduction potentials can be seen as a measure of the difference in energy levels between the HOMO and LUMO and are used to verify whether an oxidation/reduction reaction will take place on the surface of a semiconductor (Fig. 2.6).[48, 79-81] Another option is to remove the e^- to an external circuit and use the electric current for work or store the generated potential in a battery.[48, 82]

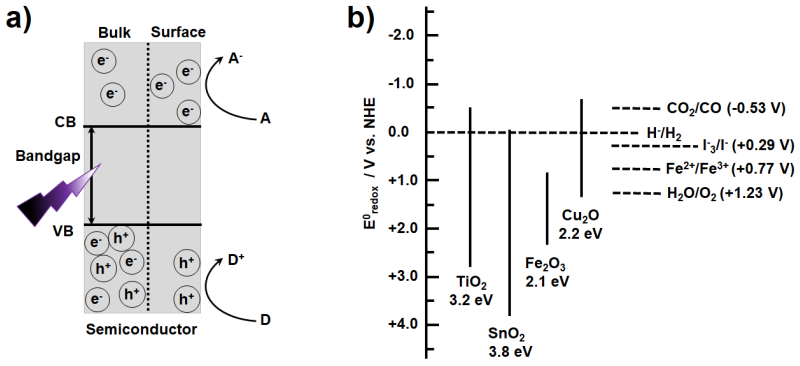

Figure 2.6. (a) Schematic representation of semiconductor photoexcitation and electron transfer on its surface. **(b)** Bandgap of some semiconductors and examples of redox potentials for some interesting reactions.

The factors that affect the efficiency of ET on the surface are related to the rate of recombination of e^- with h^+, the rate of migration of the charges to the surface, the morphology of the surface in terms of trap sites, the transfer of mass from the donor /acceptor to donate/receive electrons and if there is adsorption/desorption of these species on the semiconductor surface.[48]

3 METHODS

This chapter presents a summarized description of the main spectroscopic methods used in this work.

3.1 Steady State Absorption Spectroscopy

3.1.1 Ultraviolet-Visible Absorption

The starting point of photophysical characterization is to verify which wavelengths a molecule absorbs and how strong the absorbance is. A spectrophotometer is used to obtain an absorption spectrum. The equipment contains a lamp, which emits light in the UV-Vis region; a monochromator, which contains a dispersing element that separates light into different wavelengths; and a detector (Figure 3.1). The detector evaluates the light intensity before (I_0) and after (I) passing through the sample, the attenuation of the intensity is the measure of absorption. The result is shown in a plot of the intensity of light absorbed versus the measured wavelength.

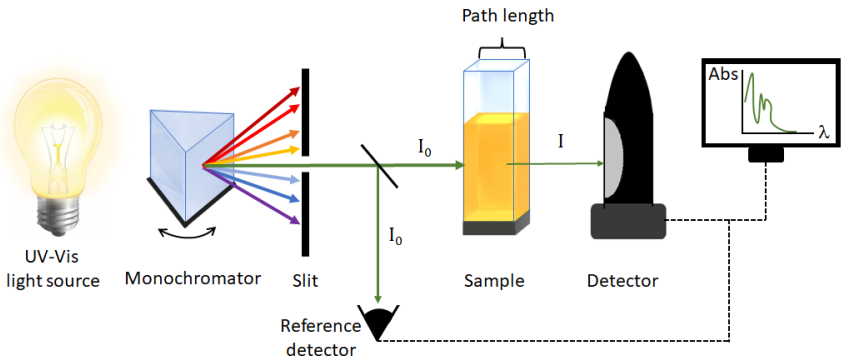

Figure 3.1. A schematic illustration of an absorption spectrophotometer.

The intensity of the transmitted light depends on the concentration (C) and the path length (l). For low concentrations the absorbance (Abs) is described by the Beer-Lambert law (Eq. 3.1).[38]

$$Abs = \varepsilon Cl \tag{3.1}$$

where ε is the molar absorption coefficient and its magnitude is a measure of the attenuation of light at a given wavelength.

In the works presented here, a Dual Beam UV-Vis Varian Cary 50 Bio Spectrophotometer was used.

3.1.2 Steady State Absorption Coupled Photolysis

Photophysical and photochemical processes can be accompanied by changes in the absorption spectrum of a molecule or material. To observe the changes, an external

excitation source is added to the spectrophotometer described above, at a right angle with respect to the lamp of the spectrophotometer. This source can be a UV-Vis broadband lamp, or a monochromatic light emitting diode (LED) or a laser. As the sample is continuously irradiated, differences in the absorption spectrum are measured over time.

Figure 3.2 illustrates the set-up used to observe the changes in the absorption spectrum of electrons in the conduction band of TiO_2 thin films. The cuvette containing the film was placed inside the spectrophotometer, as described in Section 3.1.1, and an external excitation source was used to photoexcite the film. In the case of photoexcitation with the TTA-UC fluorescence emission, a second cuvette was used, and it was placed in close proximity of the cuvette with the TiO_2 film. A 405 nm continuous wave diode laser (Coherent OBIS, 0.08 mm beam diameter) was used to excite the TTA-UC cuvette. Control experiments were carried out by photoexcitation of the TiO_2 film with a 365 nm LED. In this case, between the LED and the cuvette with the film, a neutral density filter was placed to change the power of the excitation and a lens was used to reduce the illuminated area (diameter ~ 3 mm).

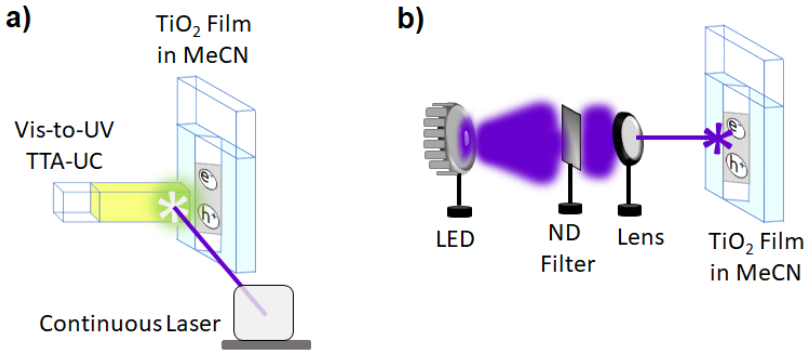

Figure 3.2. Schematic illustration of the photoexcitation of TiO_2 film with **(a)** TTA-UC fluorescence emission and **(b)** with a LED light source. MeCN stands for acetonitrile.

3.2 Transient Absorption Spectroscopy

Excited states also absorb light, and this can be used to study the properties of the excited states that are non-emissive. Our set-up consists of a Quanta-Ray Nd:YAG nanosecond pulsed laser (10 ns pulse, 10 Hz repetition rate), a continuous UV-Vis lamp, a monochromator (Oriel Cornerstone), a detector (Applied Photophysics 5 stage photomultiplier tube - PMT). The detector can be a camera containing a charge-coupled device (CCD), to obtain an absorption spectrum, or a PMT to obtain excited state kinetics. The layout of the set-up is shown in Figure 3.3-a.

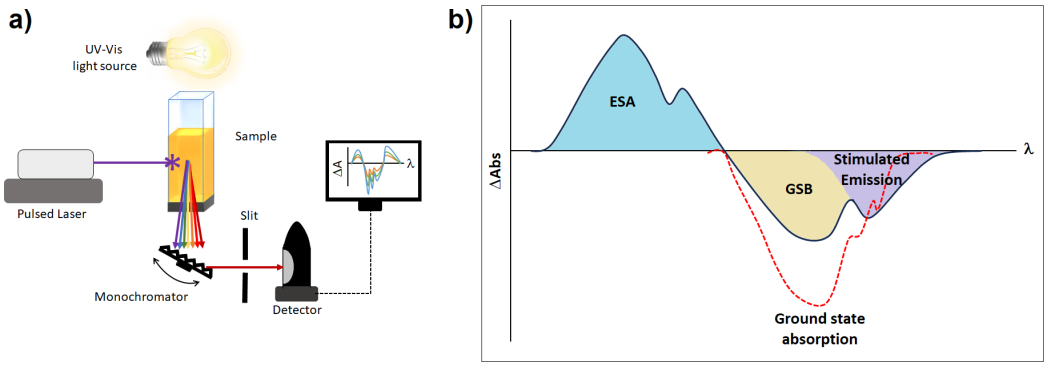

Figure 3.3. (a) Schematic illustration of the transient absorption set-up. **(b)** Example of the different signals (filled regions) in the transient absorption spectrum. The dashed red line is the ground state absorption spectrum.

The Beer-Lambert law is applied for the attenuation of the UV-Vis lamp signal before and after the laser. Without laser excitation, the probe signal intensity refers to the ground state absorption. With laser excitation, the ground state absorption decreases because the molecules were promoted to the excited state, and a new signal is detected due to the excited state absorption. The result is presented as differential absorption, ΔAbs (Eq. 3.2).[83] In the transient absorption spectrum (Fig. 3.3-b), the negative signals are related to depletion of population in the ground state, or ground state bleach (GSB), and stimulated emission. The positive signs are related to the molecules absorbing light in the excited state (ESA).

$$\Delta Abs = Abs_{with\ laser} - Abs_{without\ laser} \tag{3.2}$$

The same set-up, but without the probe light, was used for time-resolved emission to measure lifetimes in the range from 10 ns to 10 ms.

3.3 Steady State Emission

The spectrum of the radiative decay of an excited molecule is also obtained with a spectrophotometer, however, the detector is placed in right angle relative to the excitation light (Fig. 3.4-a). The apparatus has two monochromators. Choosing only one wavelength to excite the sample, in the monochromator located before the sample, an emission spectrum can be measured with the monochromator after the sample. The equipment used here is a Varian Cary Eclipse Fluorescence Spectrophotometer or a Fluorolog-3 Spectrofluorometer from Horiba Scientific.

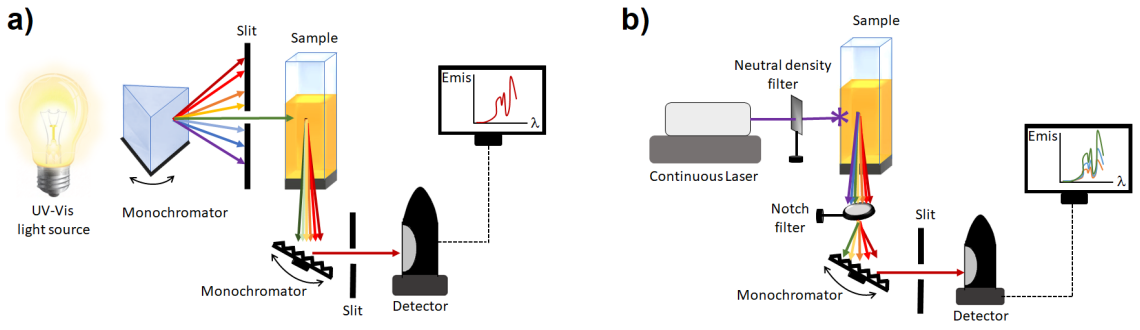

Figure 3.4. Schematic illustration of **(a)** an emission spectrophotometer and **(b)** the TTA-UC emission set-up

To study the TTA-UC emission a home-built set-up was used (Fig. 3.4-b). It contains as excitation light a monochromatic continuous wave Coherent OBIS diode laser (λ_{ex} = 532 nm, 0.07 mm beam diameter, and λ_{ex} = 405 nm, 0.08 mm diameter), an emission monochromator, and a PMT detector. Between the laser and the sample, a neutral density filter was placed to allow for variation in the excitation power. To reduce the intensity of the laser signal in the emission spectrum, a notch filter was placed between the sample and the monochromator.

3.4 Time-Correlated Single-Photon Counting

The Time-Correlated Single-Photon Counting (TCSPC) set-up used to measure the emission lifetimes from 700 ps to 30 µs uses a monochromatic pulsed laser as excitation source. In the monochromator after the sample a single wavelength is selected at which the decay is measured.

The TCSPC technique is very sensitive for detecting a single photon emitted by the sample after being excited by a laser pulse. A part of the laser light is separated and used as a signal to start timing in a stopwatch. The other part of the laser light is directed towards the sample. After excitation, the sample remains in the excited state for a certain time until the emission of photons. The first photon that reaches the detector stops the stopwatch. This cycle is repeated and the time between excitation and emission is accumulated in a multi-channel analyzer. The decay is shown in a histogram. The instrument response function (IRF) is deconvoluted from the emission decay. The IRF is measured using a scattering sample in the same conditions as the test sample.[38]

Here the TCSPC was performed in an Edinburg Instruments fluorescence Spectrometer with PicoQuant picosecond laser diodes.

4 PHOTON UP- AND DOWNCONVERSION IN SELF-ASSEMBLED ORGANOGELS

TTA-UC and SF occur through the mechanism of Dexter photo-induced energy transfer. Consequently in solution they rely on the relative position between the chromophores, for good electronic coupling, and the lifetime of the excited state.[62]

In liquid solution for some of the most successful TTA-UC systems the efficiency reaches 38% (out of maximum 50%).[84] This is because the sensitizer and the annihilator are free to diffuse and interact for energy transfer. A common practice is that the concentration of the annihilator is higher than that of the sensitizer. This increases the possibility of efficient triplet energy transfer and triplet-triplet annihilation. However, if there is a possibility of the TTA-UC system to re-absorb the UC emission, it is necessary to find a concentration that minimize it.[19, 85, 86] Performing TTA-UC in solid state can no longer rely on diffusion and this may hamper efficiency. The high concentrations of the chromophores to ensure proximity for energy transfer may bring up other energy loss channels, such as back energy transfer from the annihilator to the sensitizer,[87-89] and the sensitizer can undergo TTA (s-TTA) returning the energy to its singlet excited state.[90, 91]

On the side of SF, it requires high concentration of chromophores in liquid solution as the singlet excited state decay is usually faster than diffusion.[68, 92, 93] A common practice to ensure favorable electronic coupling for SF in solution is to covalently bind the chromophores as dimers.[69, 71, 94-96] Otherwise, the crystalline state is preferable to promote strong exciton coupling.[93, 97] The challenges lie in understanding the dynamics of the correlated triplet pair, the splitting into two triplets and the efficient extraction of them from the matrix in which SF is being performed.

Either way both TTA-UC and SF should preferably be realized in solid state so that they can be used in practical devices. Self-assembly soft materials such as polymers,[87, 90, 98-101] membranes,[102] micelles,[103-105] and gels[19, 106-109] are interesting because they allow for control of the distribution and distance between chromophores. The gels stand out due to the advantage of the formed crosslinked three dimensional (3D) network that holds a large amount of solvent, creating micro-spaces in which a solute can still diffuse.[110, 111] Usually, the chromophore is added to the gel prior to gelation.[106] Although the synthesis of gelators modified by the covalent linkage of chromophores is complex and time-consuming, optimization is valuable in order to maximize proximity and electronic coupling between the molecules to perform TTA-UC and SF.[19, 106-108, 112]

In this thesis, it was evaluated whether the self-assembly organogel formed from oxotriphenylhexanoate (OTHO),[25, 113-117] which is a low molecular weight gelator, can be used as a platform for TTA-UC and SF. OTHO gels are readily formed when a hot solution, containing the gelator and solvent, is cooled to room temperature. Through an easy synthetic route, OTHO enables the covalent incorporation of chromophores in any of its four aromatic rings (Fig. 4.1).

To test the hypothesis that chromophore-decorated OTHOs could be used for TTA-UC and SF we used the benchmark compounds, platinum octaethylporphyrin (PtOEP) as sensitizer, and 9,10-diphenylanthracene (DPA) as annihilator,[19, 25, 62, 84, 118, 119] for TTA-UC and 6,13-Bis(triisopropylsilylethynyl)pentacene (TIPS-PC) as a singlet fission chromophore.[20, 120-122] Figure 4.1 shows the molecular structures of each chromophore.

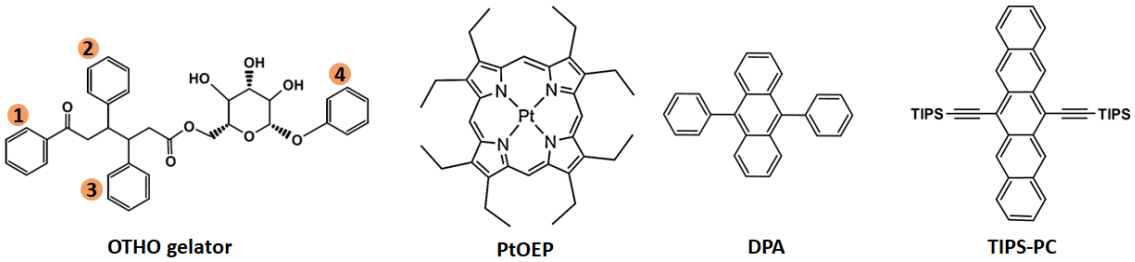

Figure 4.1. The molecular structures of OTHO gelator, the sensitizer PtOEP and the annihilator DPA used for TTA-UC, and the chromophore TIPS-PC used for SF.

4.1 OTHO Gels for TTA-UC and SF

For TTA-UC the annihilator, DPA, was covalently bound to the OTHO molecule, while the sensitizer, PtOEP, was always kept free to allow diffusion into the gel matrix, by dissolving it in the matrix prior to gelation. One hypothesis is that this configuration would allow efficient triplet energy transfer (TET) between the sensitizer and the annihilator. As the annihilator cannot diffuse, the triplet-triplet annihilation (TTA) step now becomes dependent on the exciton migration. In total three OTHO-DPA derivatives were investigated (Fig. 4.2). Two of them contain only one DPA unit attached in the *para*-position to the aryl ring #1 and #2. The other contains two DPA units, each of them was bound to the rings #1 and #2.

All three OTHO-DPA formed gels in toluene and the turbidity of the samples indicates that the fibers are of the order of 1.0 μm.[116]

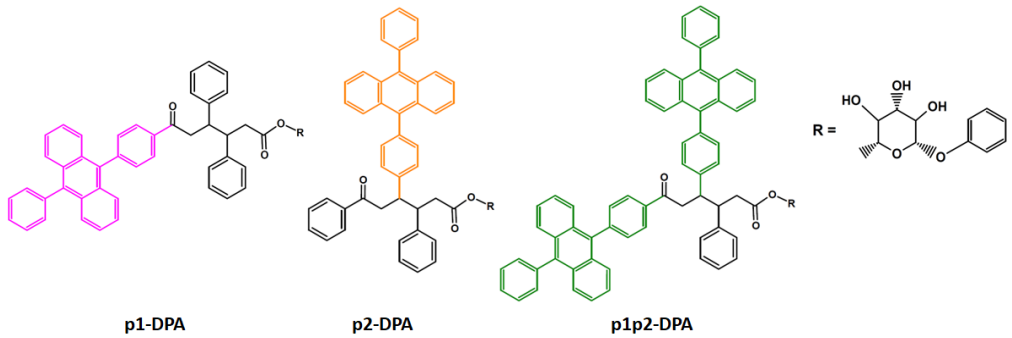

Figure 4.2. The molecular structures of OTHO-DPA derivatives. In the abbreviations the letter *p*- stands for *para*-substitution and the number refers to the aromatic ring in OTHO (see Figure 4.1).

For SF, the TIPS-PC chromophore was attached to OTHO varying the 4 aromatic rings in the *ortho*-, *meta*- and *para*-substitutions. In total 12 OTHO-PC derivatives were synthesized (Fig. 4.3), out of which ***p1-PC***, ***p2-PC***, ***m1-PC*** and ***m2-PC*** promptly formed gels at concentrations of 5 mg/mL.

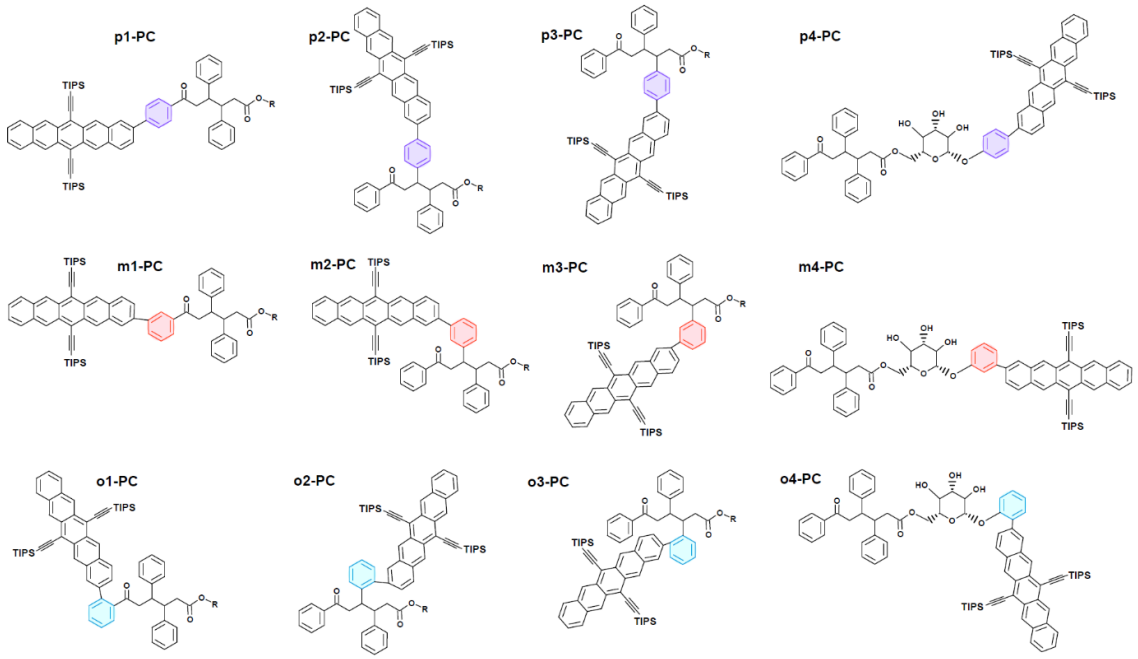

Figure 4.3. The molecular structures of OTHO-PC derivatives. In the abbreviations the letter *o*-, *m*-, and *p*- refer to *ortho*-, *meta*- and *para*-substitution and the number to the aromatic ring in OTHO (see Figure 4.1).

In summary, only *para*- and *meta*-substitutions on rings #1 and #2 of OTHO do not interfere with gel formation. Furthermore, the nature of the chromophore does not appear to control gel formation, as DPA and TIPS-PC decorated OTHOs readily formed gels. This is in agreement with literature reports.[115, 117]

4.2 Photophysical Characterization of OTHO-Chromophore Derivatives

The photophysical properties of the gels were evaluated using absorption and emission techniques. To minimize the oxygen concentration for triplet lifetime measurements, the samples were prepared in a nitrogen glovebox.

For SF only the *meta*- and *para*-substituted compounds on aromatic rings #1 and #2 of OTHO were evaluated, together with a reference sample consisting of free TIPS-PC dissolved in unsubstituted OTHO prior to gelation.

4.2.1 Steady State Absorption and Emission

When PtOEP and DPA are freely dissolved in OTHO, *i.e.* added before gelation in unsubstituted OTHO, the absorption and emission spectra (Fig. 4.4) are similar to their spectra in toluene solution. The absorption spectrum of OTHO-DPA gel derivatives is similar to free DPA in OTHO gel. The emission spectra show maximum intensity at the same wavelength as free DPA in OTHO gel, but they are broadened and do not show the vibrational structures. Therefore, the ground state properties of DPA are maintained when it is bound to OTHO.

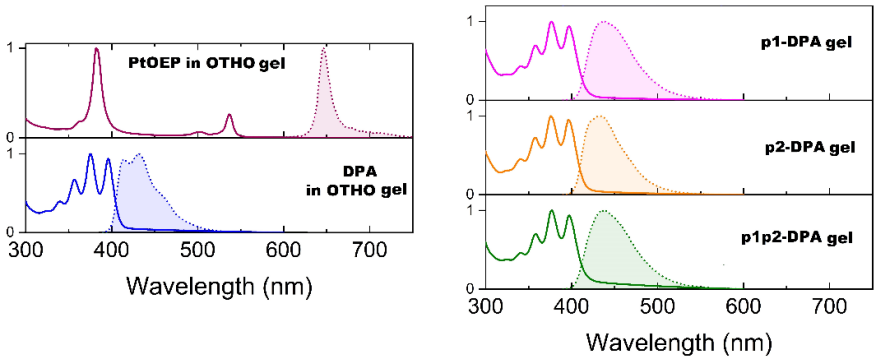

Figure 4.4. Normalized absorption and emission spectra of free PtOEP in OTHO gel (6 μM, [OTHO] = 10 mM), free DPA in OTHO gel, ***p1-DPA***, ***p2-DPA*** gels ([OTHO-DPA] = 10 mM) and ***p1p2-DPA*** gel ([OTHO-DPA] = 5 mM, [OTHO] = 5 mM).

It was not possible to determine the fluorescence quantum yield (Φ_{FA}) of OTHO-DPA gels due to light scattering, as can be seen in the tails to the red end of the absorption spectra. Therefore, Φ_{FA} was determined in very diluted toluene solutions using DPA in toluene as a reference (Φ_{FA} = 100%) according to Equation 2.4. As a result, for ***p2-DPA*** the Φ_{FA} ~ 100%, while for ***p1-DPA*** and ***p1p2-DPA*** it is around 50%. It appears that binding DPA to the aromatic ring #1 of OTHO promotes more non-radiative decay from the singlet excited state than to the #2, yet we have no clear reason for this behavior.

For TIPS-PC freely dissolved in OTHO gel the absorption and emission spectra are similar to the toluene solution (Fig. 4.5). The absorption spectrum of ***m1-PC***, ***m2-PC***, ***p1-PC*** and ***p2-PC*** gels show similar vibrational structures to TIPS-PC in OTHO gel, however the peaks are red-shifted. This has already been observed when there is aggregation or electronic coupling on the ground state.[68] Interestingly, for ***m1-PC*** gel a new absorption band around 700 nm appears during gel formation. Previous observations indicate that this could be due to strong coupling between chromophores or packing aggregation.[123] Qualitatively, the aggregation hypothesis can be approximated by analyzing the ratio between the 0-0 and 0-1 vibronic bands.[124] In diluted solution all OTHO-PC derivatives showed 0-0/0-1 lower than TIPS-PC. This decrease was reported as H-aggregation and it seems that for TIPS-PC derivatives it can also happen in diluted solution.[124]

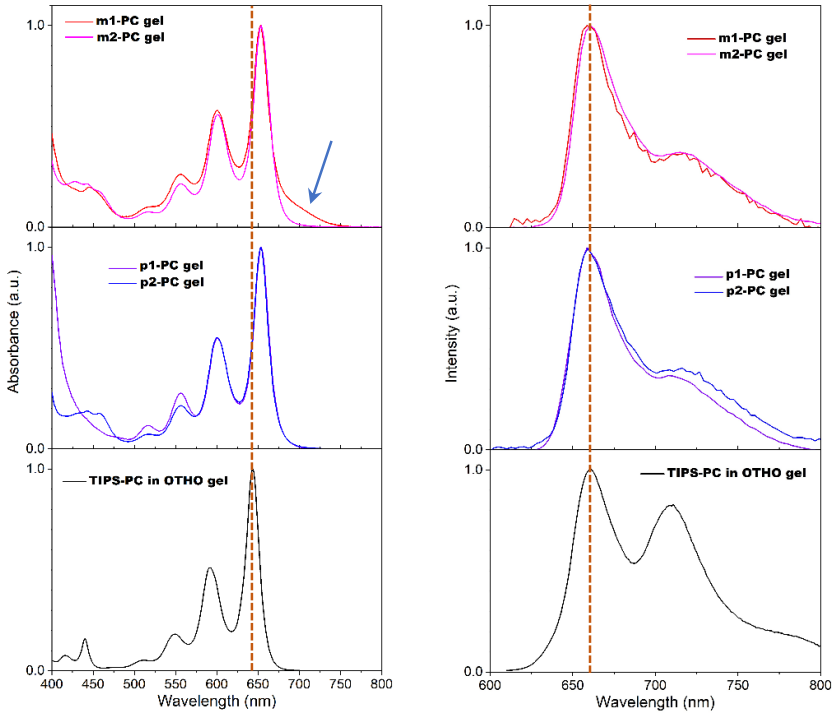

Figure 4.5. Normalized absorption and emission spectra of free TIPS-PC in OTHO gel and OTHO-PC gels (all samples 6 mg/mL). The vertical dashed lines are a guide to the eye to emphasize the shift in absorption. The arrow indicates the absorption band around 700 nm that grows in during the gelation process for ***m1-PC***.

The total internal reflection technique was used to measure the emission spectra while minimizing the inner filter effect for the TIPS-Pc samples.[92] The emission spectra of the OTHO-PC gels are unchanged in relation to free TIPS-PC in OTHO gel, presenting the similar vibrational structures with the red shift as appeared in the absorption. This indicates that there is no formation of excimers that could quench the excited state energy.

Unlike OTHO-DPA derivatives which were turbid, OTHO-PC gels appeared transparent. However, due to the high optical density it was not possible to determine the Φ_{FA} of the gel samples and they were again determined in a diluted toluene solution using TIPS-PC in toluene as a reference (Φ_{FA} = 75%). The Φ_{FA} measured for ***p1-PC*** and ***p2-PC*** was slightly less than 75%, while for ***m1-PC*** and ***m2-PC*** it was around 70%. Comparing the *para*- and *meta*-substitution, it appears that the latter favors non-radiative decay from the singlet excited state.

4.2.2 Time-Resolved Emission

The fluorescence emission of all OTHO derivative gels was measured using Time-Correlated Single-Photon Counting. The emission lifetime (λ_{ex} = 377 nm) for free DPA in OTHO gel (6.5 ns) was similar to what has been measured in liquid toluene.[125] The same behavior was observed for the fluorescence ***p2-DPA*** gel, being

monoexponential and similar to DPA in OTHO gel. It was not possible to use the monoexponential function to represent the fluorescence decay of ***p1-DPA*** and ***p1p2-DPA*** gels. Both were modeled with a biexponential function, and the mean lifetime is about half that of DPA in OTHO gel. This behavior is consistent with that of Φ_{FA}, in which the aromatic ring #1 promotes non-radiative decay when DPA is covalently bound to OTHO.

For free TIPS-PC in OTHO gel, using low chromophore concentrations (0.6 mg/mL) the emission lifetime (λ_{ex} = 560 nm) was reasonably modeled with single exponential decay (11.8 ns) similar to liquid toluene. A biexponential decay was observed when the concentration of TIPS-PC in OTHO gel was increased (6 mg/mL). Also, the fluorescence lifetime of ***m1-PC***, ***m2-PC***, ***p1-PC*** and ***p2-PC*** gels (with concentration of 6 mg/mL) was modeled with biexponential function. The intrinsic singlet lifetime of TIPS-PC (~ 12 ns) dominates the decay, while the short component is on the order of 3 to 5 ns.

4.2.3 Triplet Energy Transfer in OTHO-DPA Gels

Nanosecond spectroscopy was used to measure the phosphoresce lifetime of PtOEP in unsubstituted OTHO gel, and the decay was fitted with a biexponential function. Both at low and high concentration and excitation intensity the phosphorescence lifetime is around of tens of μs, which is shorter than in toluene solution, suggesting that sensitizer triplet-triplet annihilation (s-TTA) is happening, due to collision between two excited molecules.[126] Possibly the gel network encapsulates the solvent, forming pockets, and the concentration of PtOEP in this location will be high, promoting s-TTA. This is an energy loss pathway and may negatively affect the efficiency of the overall TTA-UC process.

To study the triplet energy transfer (TET) between the sensitizer and the annihilator, the PtOEP concentration was kept constant (115 μM) and the DPA concentration was varied between 0 and 10 mM in the gels. To obtain the desired concentration of the annihilator the gels containing ***p1-DPA***, ***p2-DPA*** and ***p1p2-DPA*** were mixed with unsubstituted OTHO. In all cases the total gelator concentration was maintained at 10 mM. The steady state and time-resolved phosphorescence emission intensity of PtOEP as a function of DPA concentration was measured (Fig. 4.6). Then the Stern-Volmer equation (Eq. 4.1) was used to evaluate the quenching capacity.[38]

$$\frac{I_0}{I} = \frac{\tau_0}{\tau} = 1 + k_{TET}\tau_0[Q] \qquad (4.1)$$

where, I_0 and I are the emission intensity without and with the quencher respectively, τ_0 and τ are the phosphorescence lifetime without and with the quencher respectively, k_{TET} is the rate of triplet energy transfer.

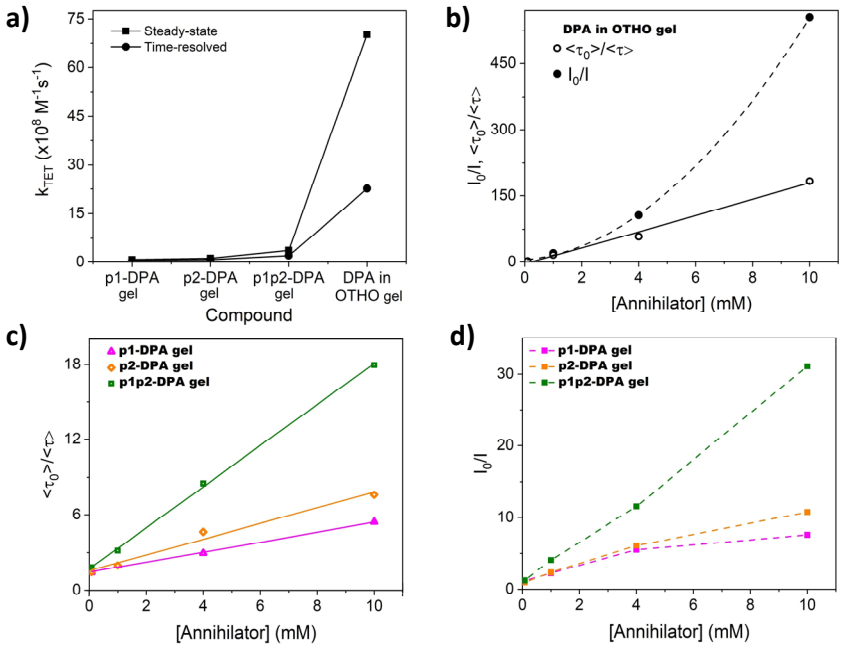

Figure 4.6. Stern-Volmer plots of PtOEP phosphorescence quenching. **(a)** Comparison of the triplet energy transfer rate in the different gels samples. **(b)** Time-resolved and steady state plots for free DPA in OTHO gel. **(c)** Time-resolved plots for OTHO-DPA gels. **(d)** Steady state plots for OTHO-DPA gels. Solid lines are linear fits, and dashed lines are guides to the eye. ([DPA units] = 0.08, 1, 4 and 10 mM, [OTHO units] = 10 mM, [PtOEP] = 115 μM)

In Equation 4.1 the average lifetime (calculated with Eq. 2.6) was used for time-resolved analysis ($<\tau_0>/<\tau>$), because the lifetime of PtOEP phosphorescence in OTHO gel has biexponential decay. For steady state plots (I_0/I) the integrated area of the phosphorescence emission was used.

The bimolecular quenching rate k_{TET} for OTHO-DPA gel derivatives is lower than for free DPA in OTHO gel (Fig. 4.6-a), indicating that in self-assembly OTHO gels the probability of the sensitizer meeting with the annihilator is reduced. The high k_{TET} for DPA in OTHO gel suggests that the matrix allows good diffusion and encounter with PtOEP. As reference, when PtOEP and DPA are in toluene solution the reported k_{TET} is 2.15×10^9 $M^{-1}s^{-1}$.[85] This behavior, of the gel providing a liquid-like environment, was previously observed by Sripathy et al., where the quench rate of PdTPP by DPA was measured in 1,3:2,4-bis(3,4-dimethylbenzylidene) sorbitol organogel.[106]

The plots with time-resolved and steady state data showed different trends (Fig. 4.6), where time-resolved data show a linear relationship, while steady state deviates from the linear behavior expected from Equation 4.1. A downward curvature, as for ***p1-DPA*** and ***p2-DPA*** gels, indicates that the quencher has limited accessibility to the fluorophore while an upward curvature indicates that static and dynamic quenching are simultaneously present when DPA is free in OTHO gel.[38] To analyze the upward curvature, Equation 4.1 is modified to calculate the dynamic (K_D) and static (K_S) quench constants (Eq. 4.2).[38]

$$\frac{I_0}{I} = (1 + K_D[Q])(1 + K_S[Q]) \quad (4.2)$$

For DPA in OTHO gel, K_S = 355 M^{-1} which represents 3% of K_D. As mentioned earlier, the small pockets of encapsulated solvent in the gel probably bring the annihilator closer to the sensitizer and cause this apparent static quenching to occur.

One way to evaluate the quenching efficiency (f_Q) by collision of PtOEP with DPA in self-assembly gels is through the Smoluchowski equation (Eq. 4.3). The parameter f_Q relates k_{TET} to the diffusion-controlled bimolecular rate constant (k_0) and allows one to investigate if the lower k_{TET} for OTHO-DPA gel derivatives is due to the attachment of the annihilator to the gel structure.[38]

$$k_0 = \frac{4\pi N}{1000}\left(R_f + R_q\right)\left(D_f + D_q\right) \quad (4.3)$$

$$D = \frac{kT}{6\pi\eta r}$$

$$f_Q = \frac{k_{TET}}{k_0}$$

where k_0 is the diffusion-controlled bimolecular rate constant, N is Avogadro´s number, k is the Boltzmann´s constant, D_f and D_q are the diffusion coefficients of fluorophore and quencher, respectively, T is the temperature (293 K), η is the solvent viscosity (toluene 0.59 mPa.s), and r is the molecular radius (PtOEP = 6.3 Å[126], and DPA = 6.55 Å – estimated using the Chemdraw3D software).

For DPA free in OTHO gel the D_q = 5.6×10^{-6} cm^2/s; while in ***p1-DPA***, ***p2-DPA*** and ***p1p2-DPA*** gels the annihilator diffusion is hindered as it is assumed that D_q = 0. A reduction of k_0 is expected for OTHO-DPA gel derivatives as there are no quencher diffusion coefficient in these systems. The results of f_Q using steady state and time-resolved data are shown in Table 4.1. The greatest quenching efficiency occurs for free DPA in OTHO gel. Among the OTHO-DPA derivatives, ***p1p2-DPA*** gel shows the highest quenching efficiency. Probably, in ***p1p2-DPA*** gel the annihilator is more accessible for quenching due to the formation of a network with narrower gel fibers. Therefore, it can be expected that it is not only the covalent binding of DPA to OTHO that causes the low k_{TET} in ***p1-DPA*** and ***p2-DPA*** gels.

Table 4.1. Quenching efficiency (f_Q) of PtOEP phosphorescence by DPA in gel matrix.

Compound	f_Q (%)	
	Steady state	Time-resolved
DPA in OTHO	64	20
p1-DPA	1.4	0.88
p2-DPA	2.1	1.4
p1p2-DPA	6.6	3.6

4.2.4 Triplet-Triplet Annihilation in OTHO-DPA Gels

To evaluate the TTA the upconverted fluorescence emission of DPA was measured by varying the excitation energy (Fig. 4.7). In the emission profiles the upconverted fluorescence appears around 432 nm and the unquenched PtOEP phosphorescence at 646 nm. Comparing the relative intensities of UC emission and phosphorescence shows that DPA in OTHO gel has a more efficient upconversion process. Among self-assembly gels, ***p1-DPA*** has the highest relative UC emission intensity indicating more efficient TTA and triplet energy migration through the gel fibers.

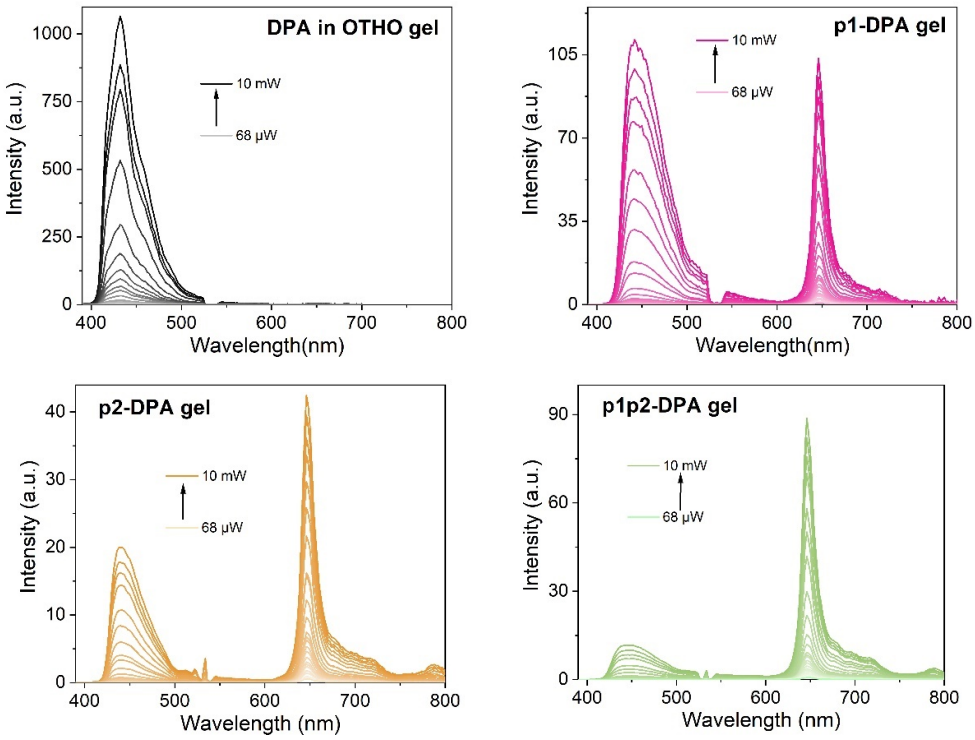

Figure 4.7. Upconverted emission profiles for various DPA samples as indicated in the panels, with excitation power varying from 68 μW to 10 mW (λ_{ex} = 532 nm) and remaining PtOEP phosphorescence at 646 nm. ([DPA units] = 10 mM, [OTHO units] = 10 mM, [PtOEP] = 115 μM)

Nanosecond time-resolved emission was used to measure the build-up of UC emission. For DPA in OTHO gel it is faster with build-up time of 45 ns, while for OTHO-DPA gel derivatives it is around 1 μs. When DPA is free to diffuse in the OTHO gel, encounters between excited annihilators are facilitated and TTA is more efficient.

With gel samples it is difficult to obtain a reliable measure of the absolute UC emission intensity due to turbidity and light scattering, and therefore the efficiency was evaluated using the intensity threshold (I_{th}) as described in Section 2.4. I_{th} values for gels samples are shown in Figure 4.8. The quadratic and linear regions were fitted with straight lines showing small deviations from the 2 and 1. This behavior is usually observed when TET is efficient. The resulting I_{th} values are high for the gels, when compared to PtOEP and DPA in toluene solution where a value of 18 mW/cm^2 was

reported.[125] It was not possible to determine I_{th} for ***p1p2-DPA*** gel using excitation power densities below 2500 mW/cm^2.

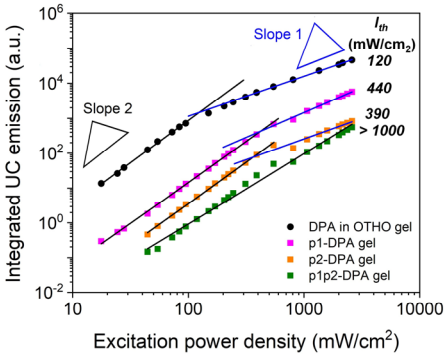

Figure 4.8. Integrated upconverted emission versus excitation power density. Black lines are linear fits with slope ~ 2 and blue line are linear fits with slope ~ 1. The I_{th} values are the crossing points between those lines. ([DPA units] = 10 mM, [OTHO units] = 10 mM, [PtOEP] = 115 μM)

The high I_{th} values indicate that the TTA step is not very efficient in the gels. The best result was obtained for free DPA in OTHO gel. As DPA cannot diffuse in the self-assembled gels, exciton migration through gel fibers is required. Although ***p1p2-DPA*** gel is less turbid and possibly forms narrower fibers that may facilitate TET, exciton migration appears to be poor and hinders TTA, resulting in a high I_{th} value. Upconversion is more efficient in ***p1-DPA*** than in ***p2-DPA*** gel, although they have similar TET. Possibly binding DPA to the aromatic ring #1 of OTHO favors exciton migration.

Reduced molecular diffusion has been invoked as explanation for other observations of high I_{th}, for example in a study by Vadrucci ***et. al.*** were they obtained I_{th} = 100 mW/cm^2 in an organogel made of poly(vinyl alcohol) and hexamethylene diisocyanate in DMSO, in which DPA and a palladium porphyrin were dissolved.[107] In contrast, there are also impressive reports using DPA and PtOEP dissolved in a N,N´-bis(octadecyl)-L-Boc-glutamic diamide gel in presence of oxygen, where a value of I_{th} = 1.48 mW/cm^2 was reported, and attributed to efficient exciton migration through the gel fibers.[108] We emphasize that the chemical synthesis to covalently link chromophores into gelators is usually arduous, which does not apply to ***p1-DPA***, ***p2-DPA*** and p1p2p-DPA which are easily produced from OTHO.

4.2.5 Triplet Formation in OTHO-PC Gels

Sensitization with PtOEP was used to determine the triplet state spectroscopic signature of OTHO-PC in toluene solution, by adding a small amount of each derivative to a solution containing the sensitizer PtOEP (no gelation was observed). Nanosecond transient absorption was used to monitor changes in the absorption spectrum (λ_{ex} = 536 nm) with time and the triplet signature was observed around 525 nm, a slight redshift compared to the triplet state of TIPS-PC in toluene solution which appears at 508 nm.[68]

In the OTHO-PC gel samples the excited state was studied using femtosecond transient absorption. Excited state absorption of free TIPS-PC in OTHO gel showed features similar to those reported for TIPS-PC in dilute toluene solutions with excited state absorption peaks at 450, 525 and 575 nm. Also, ***m1-PC***, ***m2-PC***, ***p1-PC*** and ***p2-PC*** in dilute solution showed similar behavior as TIPS-PC in solution and in OTHO gel. The transient absorption spectra of the OTHO-PC gels (6 mg/mL) were different from solution (Fig. 4.9). In ***m2-PC*** and ***p2-PC*** gels at long times (7 ns) the triplet at 525 nm appears more perceptible than the singlet (405 nm). For ***p1-PC*** gel between 425 and 625 nm the spectra were broad and featureless. For ***m1-PC*** gel the triplet signal at 525 nm is seen immediately after laser excitation. This rapid triplet formation may be resultant of singlet fission as opposed to *ISC* (12 ps).[68, 127] This peak at 525 nm appears with strong absorption after excitation of the ***m1-PC*** gel with 700 nm, which is the absorption band that appears during gel formation.

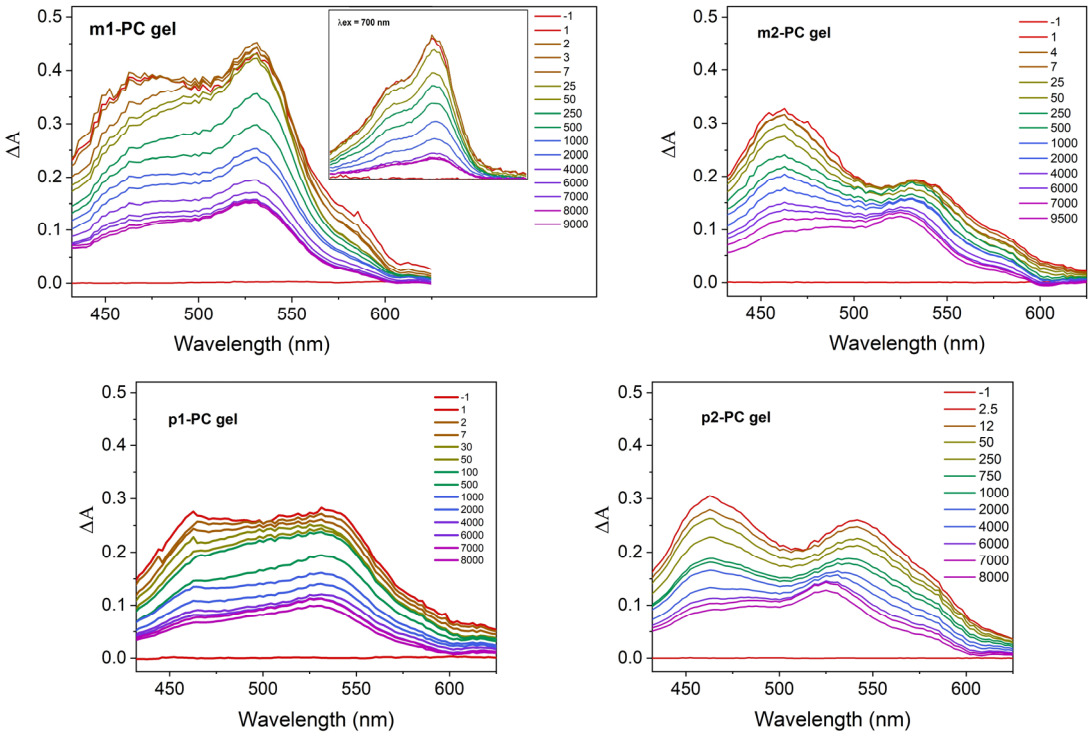

Figure 4.9 Femtosecond transient absorption spectra of OTHO-PC gels (6mg/mL, λ_{ex} = 650 nm). Inset: ***m1-PC*** gel was also excited at 700 nm. The legends show the time picosecond scale.

Nanosecond transient absorption (λ_{ex} = 653 nm) was used to study the lifetime of the triplets (Table 4.2). ***m2-PC*** and ***p1-PC*** have triplet lifetime around 28 µs, which is *ca* 10 µs shorter than TIPS-PC in solution. On the other hand, ***m1-PC*** presented the longest lifetime, around 68 µs and ***p2-PC*** 46 µs, which is almost 10 µs longer than TIPS-PC in solution. When the concentration is increased (6 mg/mL), the longer lifetime component decreased to around 25 µs for all the samples. Interestingly, ***m1-PC*** gel that could be excited at 700 nm (6 mg/mL), due to the new absorption band that appeared during gelation, the longer component of the triplet lifetime increased to 60 µs, recovering the lifetime as it was in dilute toluene solution. It can be hypothesized

that each self-assembly gel forms a different structure that affects the triplet decay, but a further investigation should be done to understand the details of this behavior.

Table 4.2. Triplet lifetimes in dilute solution and gel samples (λ_{ex} = 653 nm and 700 nm[a], nanosecond transient absorption = 525 nm). A1 is the amplitude of τ_1.

Diluted solution

	TIPS-Pc	***m1-PC***	***m2-PC***	***p1-PC***	***p2-PC***
τ_1 (µs)	38.5	67.8	28.2	28.5	46.0

Gel: 0.6 mg/mL

	TIPS-Pc in OTHO	***m1-PC***	***m2-PC***	***p1-PC***	***p2-PC***
τ_1 (µs)	30.0	4.3	3.9	7.2	2.0
τ_2 (µs)		34.0	33.6	30.8	29.1
A1 (%)		28	26	27	28

Gel: 6 mg/mL

	TIPS-Pc in OTHO	***m1-PC***	***m1-PC*[a]**	***m2-PC***	***p1-PC***	***p2-PC***
τ_1 (µs)	6.3	2.8	16.1	4.8	2.3	4.1
τ_2 (µs)	25.3	23.9	60.4	27.1	25.1	21.5
A1 (%)	42	26	64	29	31	25

4.3 Discussion

Here we have demonstrated that OTHO gels can be used as a matrix for TTA-UC and SF. The easy synthesis of self-assembling OTHO gelators allows versatility in attaching chromophores, however only *para*- and *meta*-substitutions on rings #1 and #2 form gels independent of the chromophore.

Different chromophore interactions were obtained, consequently affecting the efficiency of TET, TTA and SF. For TTA-UC only *para*-substitution was investigated. Although the quenching efficiency is low when DPA is attached on aryl ring #1, a better overall TTA-UC performance than the others was obtained. Possibly this environment provides better exciton migration.

The study of SF in the self-assembly gels showed that *meta*-substitution, again in the aromatic ring #1, resulted in the best structure for TIPS-PC to undergo SF, with a triplet lifetime that is similar to when the compound is in dilute solution. It was possible to verify that each self-assembling gel forms a different structure and affects the triplet excited state lifetime. This is important information that should be investigated in TTA-UC self-assembling OTHO gelators so that they can be improved.

The TTA-UC and SF studies in OTHO gel complement each other. Different substitution positions affect the photophysical and structural properties as well as the interaction between chromophores. For TTA-UC, the substitution of the annihilator in the gel should provide a structure with good accessibility of the annihilator to the

sensitizer, so that it can perform efficient TET, and facilitate exciton migration for efficient TTA. For SF, it would be interesting to find a way to control the type of structure the gel forms so that it is efficient, such as in the meta-substitution of ring #1 excited at 700 nm. Furthermore, it is necessary to reduce losses in the triplet lifetime to be able to harvest them. Due to the variety of results, to improve the up- and downconversion processes a better understanding of the structure of self-assembly OTHO gel is necessary.

5 PHOTOEXCITATION OF TiO_2 THIN FILMS WITH UPCONVERTED LOW ENERGY PHOTONS

Titanium dioxide (TiO_2) is an inorganic material widely used in water treatment, self-cleaning surfaces, pigment, sunscreen, solar cells, water decomposition, and much more.[13, 78, 128-133] Certainly this interest in TiO_2 is due to its non-toxic, stable and low-cost nature. More important than that are its photocatalytic properties. However, TiO_2 has a high bandgap (3.2 eV) and an absorption onset around 400 nm that requires excitation by UV photons.[130] A way to circumvent the spectral mismatch between the TiO_2 bandgap and visible light is using Vis-to-UV TTA-UC.

Here we have studied the photoexcitation of TiO_2 thin films with upconverted fluorescence emission. The TTA-UC system is composed of 2,5-diphenyloxazole (PPO) as annihilator and an iridium(III) complex (Tris[(2-(2-pyridinyl-kN)-5-(trifluoromethyl)phenyl-kC]iridium(III), in short Ir(p-CF_3-ppy)$_3$), in oxygen free acetonitrile solution. Figure 5.1-a shows the molecular structures of the annihilator and sensitizer.

5.1 Photophysical Characterization of the Sensitizer and Annihilator

In TTA-UC, among the requirements for the annihilator, it is necessary to have a high quantum yield of fluorescence and also that the emission coincides with the TiO_2 bandgap (below 400 nm – Fig. 5.1-b). PPO is a good candidate since its Φ_{FA} = 82% in acetonitrile and the emission peak is at 363 nm (Fig. 5.1-c) and was selected after investigation of several potential annihilators. For the sensitizer, high absorption of visible light, a long-lived triplet state with energy equal or slightly higher than that of the30nnihilateor are desirable. Ir(p-CF_3-ppy)$_3$ is a commercially available iridium(III) complex that absorbs light below 500 nm (Fig. 5.1-d), its triplet state energy is around 2.4 eV (determined from the phosphorescence emission peak at 507 nm) which is the same energy of the triplet state of PPO.[134] The phosphorescence lifetime is 2.7 μs and Φ = 60% in oxygen free acetonitrile.

It can be observed that the sensitizer absorbs photons in the PPO emission region and there is some overlap between the absorption and emission spectra of the PPO. Probably the re-absorption of emitted photons will be detrimental to the quantum yield of the UC emission.

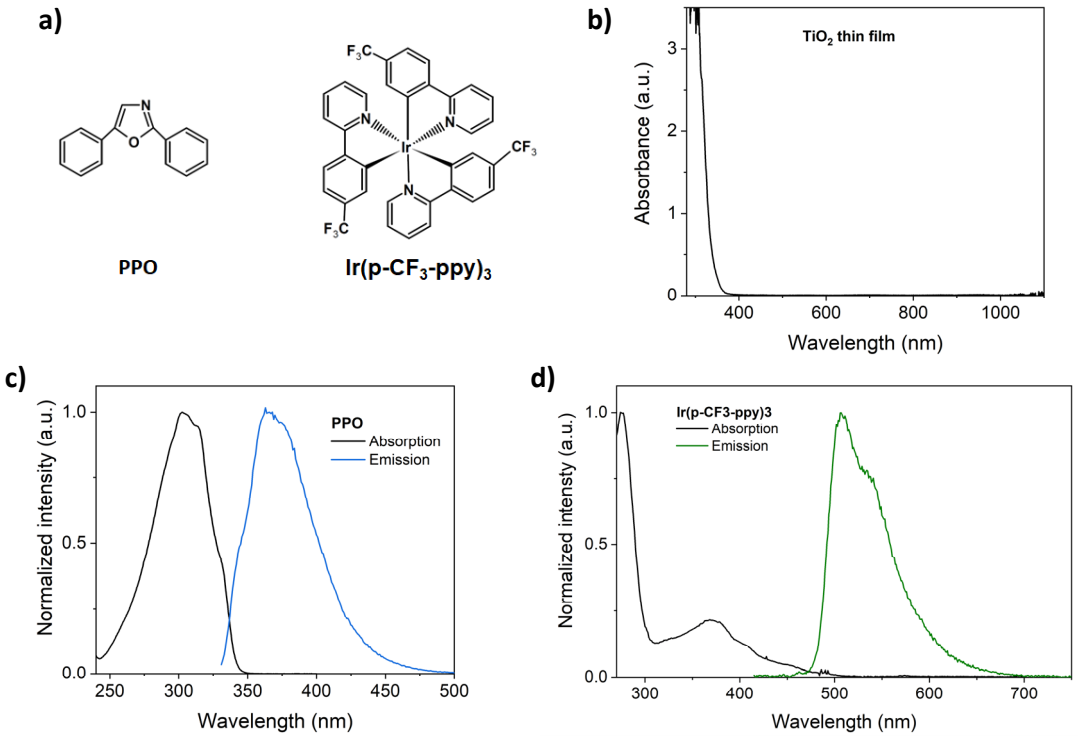

Figure 5.1. (a) The molecular structures of the annihilator PPO and the sensitizer Ir(p-CF_3-ppy)$_3$. **(b)** The absorption spectrum of TiO_2 film immersed in acetonitrile and methanol. **(c)** Normalized absorption and emission spectra, in acetonitrile, of PPO **(d)** Normalized absorption and emission spectra, in acetonitrile, of Ir(p-CF_3-ppy)$_3$.

5.2 Evaluation of Blue-to-UV Triplet-Triplet Annihilation Upconversion

When 100 μM Ir(p-CF_3-ppy)$_3$ and 15 mM PPO are together in acetonitrile solution, excitation at 405 nm results in delayed and long lived (77.8 μs) upconverted fluorescence emission with a peak at 365 nm (Fig. 5.2-a). The concentrations were chosen to minimize the secondary inner filter effect and the observed Φ_{UC} is 8.6% (maximum 50%, since one high energy photon is obtained from two photons of low energy) at 637 mW/cm^2 (Coumarin 153 in air saturated ethanol, Φ = 53%, was used as reference). The minimum excitation intensity for TTA to be dominant in the system is I_{th} = 65 mW/cm^2 (Fig. 5.2-b). Possibly a higher concentration for the sensitizer would reduce the I_{th} value, however it would increase the re-absorption of UC emission.

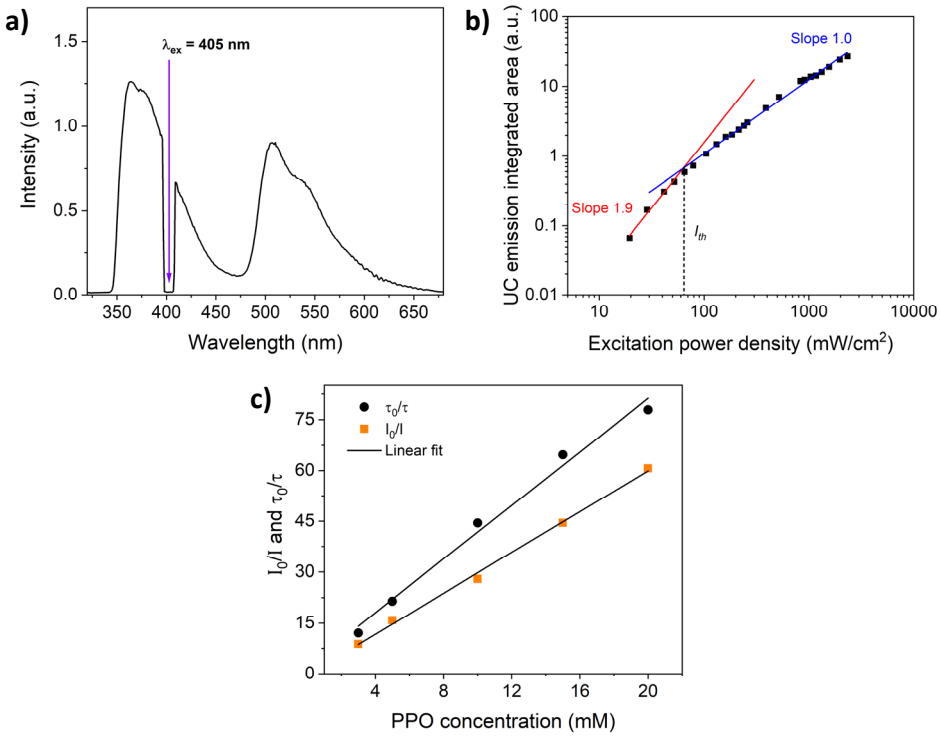

Figure 5.2. (a) Emission spectra with UC fluorescence at 365 nm and unquenched sensitizer phosphorescence at 507 nm. (λ_{ex} = 405 nm, [PPO] = 15 mM, [Ir(p-CF_3-ppy)$_3$] = 100 μM, in oxygen free acetonitrile). **(b)** Log-log plot of UC emission integrated area *vs.* excitation power density, the quadratic and linear regimes of the emission are represented by the linear fittings with slopes 2 and 1, respectively. The cross point is the intensity threshold I_{th}. **(c)** Stern-Volmer plots for steady state and time resolved data respectively.

There is still remining phosphorescence at 507 nm from unquenched sensitizer. Maintaining constant concentration for the sensitizer (100 μM), the phosphorescence quenching was analyzed with the Stern-Volmer equation (Eq. 4.1). Both steady state and time resolved plots showed linear relationship with PPO concentration (Fig. 5.2-c) and the triplet energy transfer rate is k_{TET} = 1.1×10^9 M^{-1}s^{-1}. Although this rate is almost 20 times lower than the diffusion limit in acetonitrile,[135] it is still a high rate for the annihilator to quench the triplet energy from the sensitizer. There is no indication of self-quenching since the spectrum and lifetime of phosphorescence at low and high concentrations of the sensitizer are the same. The remaining phosphorescence observed in the UC system may be the result of the secondary filter effect or sensitizer instability, as experiments showed photodegradation of the iridium compound.

Harada et al. reported Φ_{UC} = 10.2% and I_{th} = 1.1 mW/cm^2 (λ_{ex} = 445 nm) with TIPS-Naphthalene as annihilator and an iridium complex as sensitizer in deaerated THF. The good performance of this TTA-UC was attributed to the low re-absorption of UC emission.[136] A high generated $\Phi_{UC,g}$ = 14% (which account for secondary inner filter effect) with I_{th} = 210 mW/cm^2 (λ_{ex} = 405 nm) using PPO as annihilator and 2,3,5,6-tetra(9H-carbazol-9-yl)benzonitrile (4CzBN) as sensitizer, in oxygen free toluene, was reported by Olesund et al. The high I_{th} value was resultant from degradation of the

sensitizer.[67] Murakami et al. presented a stable TTA-UC in hexane constituted of 10-butyl-2-chloro-9(10*H*)-acridinone as the sensitizer and 2,6-di-*tert*-butylnaphthalene as annihilator. The Φ_{UC} was 4.1%, however I_{th} was extremely high, 1.3 W/cm^2, due to the low absorbance of the sensitizer. They claimed that the photostability takes into account the energy difference of the orbital levels of the sensitizer, annihilator and solvent, and the double electron transfer between the molecules.[137] Although the pair PPO and Ir(p-CF_3-ppy)$_3$ is not great for TTA-UC Vis-to-UV, and one ideally would have excitation at longer wavelength, it fulfills the requirements for the purpose of photoexcitation of TiO_2 thin films and testing its reactivity.

5.3 Photoexcitation of TiO_2 Thin Films with Upconverted Emission

For excitation of the TiO_2 film with TTA-UC fluorescence emission, a set-up using two cuvettes was developed, Figure 3.2 in Section 3.1.2 shows the schematic illustration for both set-ups. The absorption spectrum of the film was monitored throughout the excitation time. When the absorbance had reached its maximum, the excitation light was turned off.

When the TiO_2 film is excited with the TTA-UC emission ([Ir(p-CF_3-ppy)$_3$] = 100 μM, [PPO] = 15 mM, λ_{ex} = 405 nm, 50 mW or 9947 mW/cm^2), initially, a change in absorbance is observed between 350 and 500 nm. Over time the absorbance increases, reaches a maximum, and also broadens from 350 to 1000 nm (Fig. 5.3). The absorption band between 350 and 500 nm is reported to be due to holes, $TiO_2(h^+)$.[138] The broadest band is the conduction band electron absorption, $TiO_2(e^-)$,[138] and its absorbance (signal at 700 and 900 nm) decreases faster than the $TiO_2(h^+)$ (at 400 nm). Comparing with direct excitation using the 365 nm LED (beam diameter ~ 3 mm), the same behavior is observed when the excitation power is about 43 μW (0.61 mW/cm^2). The difference is that it takes longer to reach maximum absorbance and it is maintained for some time before it starts to decrease (Fig. 5.3). Increasing the LED excitation power to 300 μW (4.2 mW/cm^2) and 1.6 mW (22.6 mW/cm^2), the absorption is immediately present over the whole range 400-1000 nm (Fig. 5.3).

Although the maximum absorption remains for some time, when high excitation power is used with the LED, rapid recombination still occurs contrary to what has already been reported, that the electrons in the conduction band of TiO_2 remain for weeks[139] and low excitation power results in slow recombination.[138, 140, 141] Here it may be that the structure of the film, particle size, number of trap sites, or surface crystallinity are responsible for the rapid recombination.[139, 142-145]

Although the experimental design used here requires improvements for TiO_2 film to absorb more photons from UC emission, it allows for versatility. The UC system can be easily changed in the cuvette, the sensitizer and annihilator pair or the solvent can be different. The cuvette can also be replaced by a solid matrix that serves as a platform for TTA-UC. In the literature it is possible to find different examples of cell design. Khnayzer et al. reported the current generated when tungsten oxide (WO_3) with UC emission at 432 nm. They built a photochemical cell formed with a quartz cell filled with water, electrolytes, the WO_3 photoanode, a platinum cathode and the

cuvette for TTA-UC. The latter was excited with a xenon lamp, in which a long-pass filter was used to allow only wavelengths above 500 nm.[146] Barawi et al. have used a similar design, the difference is that the photoanode was a TiO_2 film excited with UC emission at 370 nm. The film was placed very close to the UC cuvette that was excited with a 445 nm laser. They have measured the produced current, the potential and the hydrogen production.[34] Another example using TiO_2 as photoanode was reported by Li et al., where they have built a dye sensitizer solar cell and TTA-UC was performed in solid-state in a polyurethane matrix. They observed increased photocurrent when a reflector is used together with the TTA-UC film.[99]

In addition to the versatility provided by the set-up used here, instead of producing electrical current as in the previous examples, the cuvette containing the TiO_2 film can be used to perform chemical reactions using the electrons and holes on its surface.

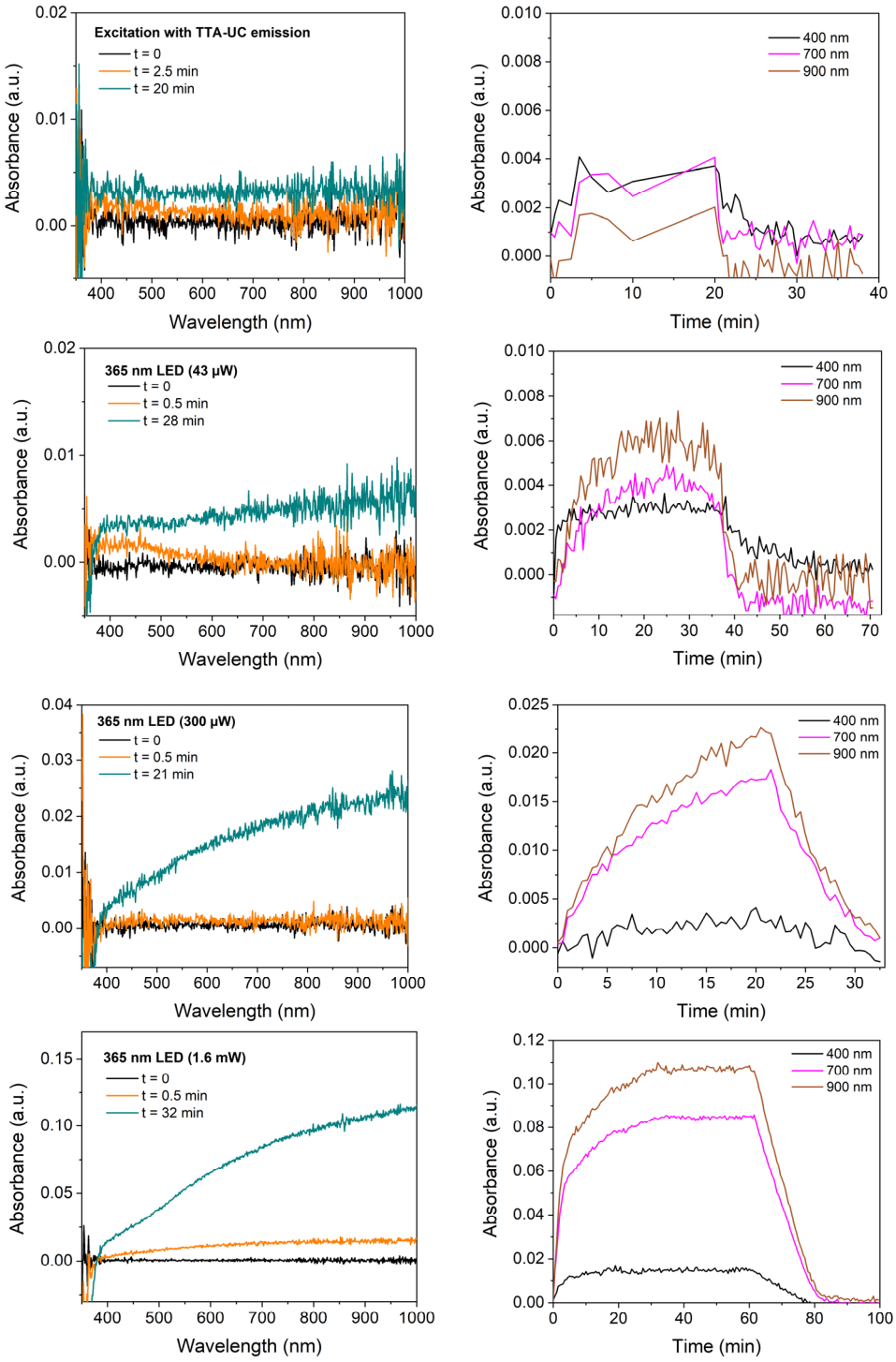

Figure 5.3 Left: UV-Vis absorption spectra of the TiO_2 film as function of excitation power. The film was excited with TTA-UC emission and with the 365 nm LED with different excitation power (43 µW, 300 mW and 1.6 mW). **Right:** Absorbance dependence with time for different wavelengths representing the region assigned to $TiO_2(h^+)$ (400 nm) and $TiO_2(e^-)$ (700 nm and 900 nm).

5.4 TiO_2 Reactivity Following TTA-UC Excitation

To test the reactivity of the holes generated by photoexcitation TiO_2 thin film with the UC emission, the iodine/iodide pair (I_2/I^-) was used. The procedure consists of placing the film in a cuvette containing a solution of lithium iodide (LiI) in acetonitrile purged with argon. The triiodide ion (I_3^-), originating from the oxidation of I^- (Eq. 5.1), has UV-Vis absorption and its formation can be monitored during the photoexcitation of the film.[147] The pair I_2/I^- is usually used as a redox mediator in sensitized dye solar cells because it has good solubility, low visible light absorption, and slow recombination with $TiO_2(e^-)$.[148-151]

$$2\,I^- + 2\,TiO_2(h^+) \leftrightarrow I_2 \qquad (5.1)$$

$$I_2 + I^- \leftrightarrow I_3^-$$

The TiO_2 film in LiI solution, now without methanol, was photoexcited with UC emission for 60 min. Changes in the absorption of the TiO_2 film were observed in the range 350-450 nm, with a peak at 365 nm, and the characteristic absorption of electrons in the TiO_2 film between 350 and 1000 nm was not observed (Fig. 5.4-a). The change in absorption with a peak at 365 nm is indicative of the formation of the I_3^- ion.[147] When photoexcitation of the film was stopped, the absorbance at 365 nm decreased and reached a plateau (Fig 5.4-b).

The absorption of the TiO_2 film, in air, was evaluated before and after excitation and showed no changes, indicating that no species was adsorbed on the surface (Fig. 5.4-c). The absorption of the LiI solution was also analyzed and it was observed that after excitation the absorption spectrum changed with an increase in absorbance at the 300 and 365 nm peaks, which are related to I_3^- (Fig. 5.4-d).

Instead of using UC emission excitation, the LiI solution film was excited with the 365 nm LED (60 μW) and the same behavior was observed. A control experiment exciting only the LiI solution, without the TiO_2 film, shows that there is no change in the absorbance of the peak at 365 nm. Therefore, the formation of I_3^- occurs only when I^- is oxidized by the holes in the TiO_2 film.

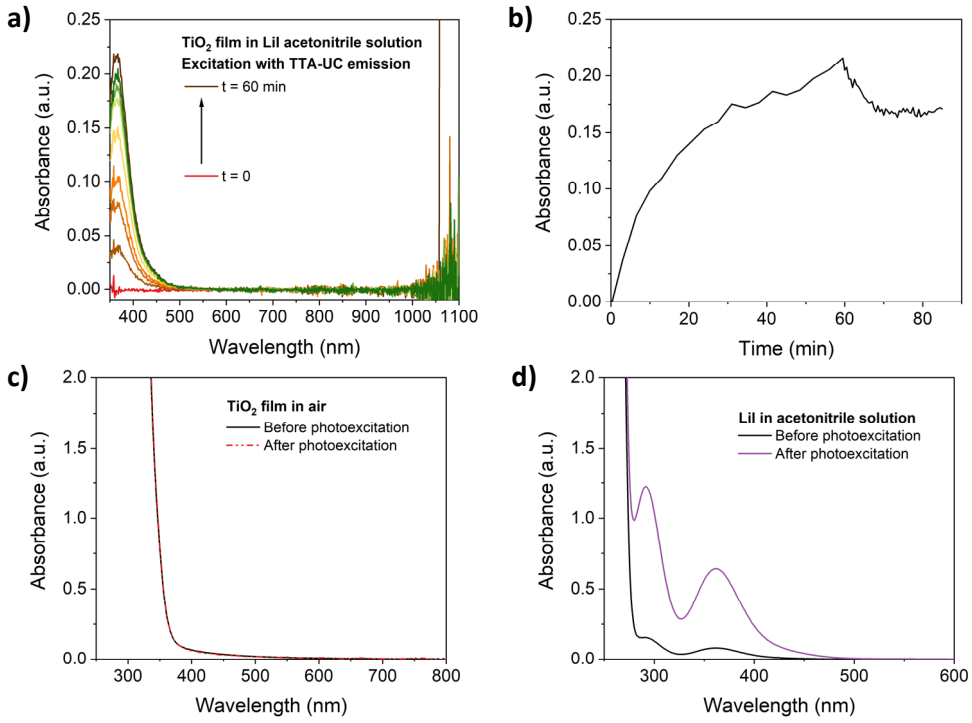

Figure 5.4. (a) UV-Vis absorption of TiO_2 film in LiI acetonitrile during photoexcitation with UC emission. **(b)** Absorbance profile at 365 nm with time. **(c)** Absorption before and after photoexcitation with the UC fluorescence emission for TiO_2 film in air. **(d)** Absorption for the LiI solution before and after photoexcitation of TiO_2 film with the UC emission.

Using the Beer-Lambert law (Eq. 3.1) and the I_3^- maximum absorbance (l = 0.2 cm, ε = 11000 $M^{-1}cm^{-1}$)[147], it is possible to calculate the concentration of $TiO_2(h^+)$, which results in $4.9x10^{-5}$ M. This concentration has the same order of magnitude as the one reported by Ito and Meyer and was used in pollutant reduction reactions in methanol and water[78] suggesting that Vis-to-UV TTA-UC can be utilized to circumvent the spectral mismatch.

5.5 Discussion

Here a positive result of the photoexcitation of TiO_2 film with TTA-UC Vis-to-UV emission was shown. The electron absorption signal, in the TiO_2 conduction band, is similar when the film is directly photoexcited by a 365 nm LED at a power intensity of 46 μW. The low excitation intensity from UC emission makes it possible to observe, initially, at the beginning of the photoexcitation, the absorption of holes (350 to 500 nm) and over time the absorption of electrons (350 to 1000 nm). Furthermore, when the absorbance is monitored at 400 nm, in the region attributed to $TiO_2(h^+)$, the decay is slower compared to the absorbance at 900 nm, in the $TiO_2(e^-)$ region. A hole concentration of almost 50 μM is produced when the TiO_2 film is excited with UC emission.

6 TWO-PHOTON ABSORPTION IN CARBON NITRIDE QUANTUM DOTS

Another way to circumvent spectral mismatch is two photon absorption (2PA). This chapter concerns 2PA properties within carbon nitride quantum dots (CNQDs). The motivation for this interest is that these quantum dots have shown promise both as photocatalysts[51, 152] on their own and as sensitizers for molecular catalysts[44]. Being able to extend the absorption out in the infrared (IR) could then be of importance for applications. Another area of great interest is the application of 2PA in fluorescence microscopy of biological tissues, since visible light has small penetration depths due to scattering or absorption of the different molecules that compose the tissue. To circumvent these difficulties, IR light, which has a greater penetration depth, can be used with the 2PA technique. Another technical advantage emerges as the excitation light is precisely focused, confining emitted fluorescence to a small area, improving resolution by reducing background.[42, 55, 153]

In biological microscopy, dyes should be water-soluble, photostable, non-toxic and have a high cross section (σ), which is the capacity to absorb photons in the 2PA regime. Here, QDs are a good option because high σ can often be obtained and the synthesis routes are often easier than for molecules with large cross sections.[42, 55, 154]

In this thesis, the photophysical characterization for 2PA was done in CNQDs, functionalized with ethylenediaminetetraacetic acid (EDTA) so that the surface becomes negatively charged, to improve solubility and allows for binding of photocatalysts.[44] The CNQDs were synthesized using a microwave-assisted approach.[155-157]

6.1 Photophysical Characterization of the Quantum Dots

Basic photophysical characterization using 1PA of CNQDs in water was carried out at room temperature, to provide comparisons for the 2PA studies. The UV-Vis absorption spectrum is shown in Figure 6.1. For this type of QDs, the absorption band is attributed to the $\pi \rightarrow \pi^*$ transitions of the C=C and C=N bonds from the tri-s-triazine rings. The shoulder observed at 335 nm is due to the $n \rightarrow \pi^*$ transition of the C=O and C=N bonds.[158-160] Using a Tauc plot, and assuming indirect bandgap, the estimated bandgap is approximately 2.4 eV.

Photoluminescence presents the characteristic behavior of QDs, which is wavelength-dependent emission (Fig. 6.1). The photoluminescence in CNQDs is attributed to the transitions with the nitrogen lone-pair of electrons with the π^* orbitals of carbon in the C=N from the tri-s-triazine rings.[160, 161] The emission lifetime was measured using TCSPC and the amplitude-weighted average lifetime was 3.9 ns. The emission quantum yield was determined to be 3.8% using Coumarin 102 (Φ = 76% in air saturated ethanol) as reference. The photophysical behavior for 1PA found here is in agreement to what has already been reported in the literature for CNQDs.[162]

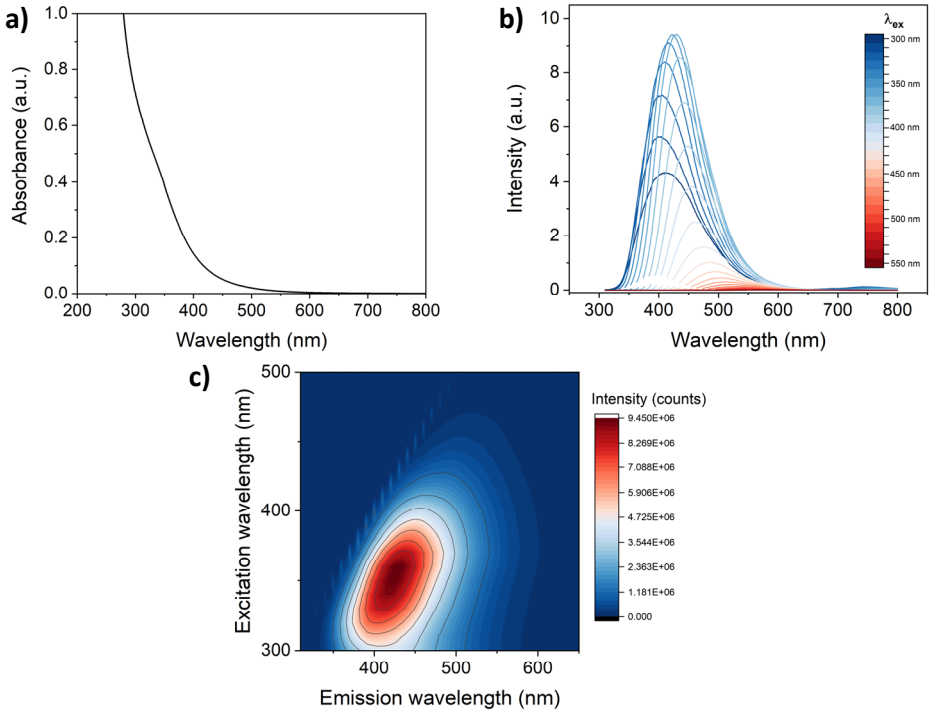

Figure 6.1 (a) UV-Vis absorption spectrum of the CNQDs in water. **(b)** 1PA emission spectra dependent on the excitation wavelength. **(c)** 3D emission spectra.

6.2 Two-Photon Absorption

A detailed study of the 2PA behavior, using a fluorescence microscope equipped with a femtosecond laser (100 fs pulse, repetition frequency 80 MHz) was carried out. Using this set-up, it was possible to evaluate the emission intensity with excitation power, between 680 and 860 nm (with increments of 10 nm), Figure 6.2. No generation of white light was observed when only water without CNQDs was tested.

By varying the power, quadratic behavior of the emission was observed at all wavelengths. In a plot of the logarithm of the emission intensity *versus* the logarithm of the excitation power, this behavior is described by linear fitting with slope 2. When the fitted slope results in 1 the relationship is purely linear, and the emission intensity is proportional to the absorption that occurs due to 1PA. Slope values greater than or equal to 1.8 are typically considered purely 2PA.[163] Therefore, when the slope is between 1 and 1.8, both 1PA and 2PA can occur simultaneously.[55] Other processes, such as stimulated emission, absorption and saturation of the excited state, intensity-dependence of the 2PA cross section, may be responsible for the deviations in the slope values and this depends on each type of system.[164] Here, for the CNQDs, the average value of the slopes is about 1.97, being characteristic of the pure 2PA process.

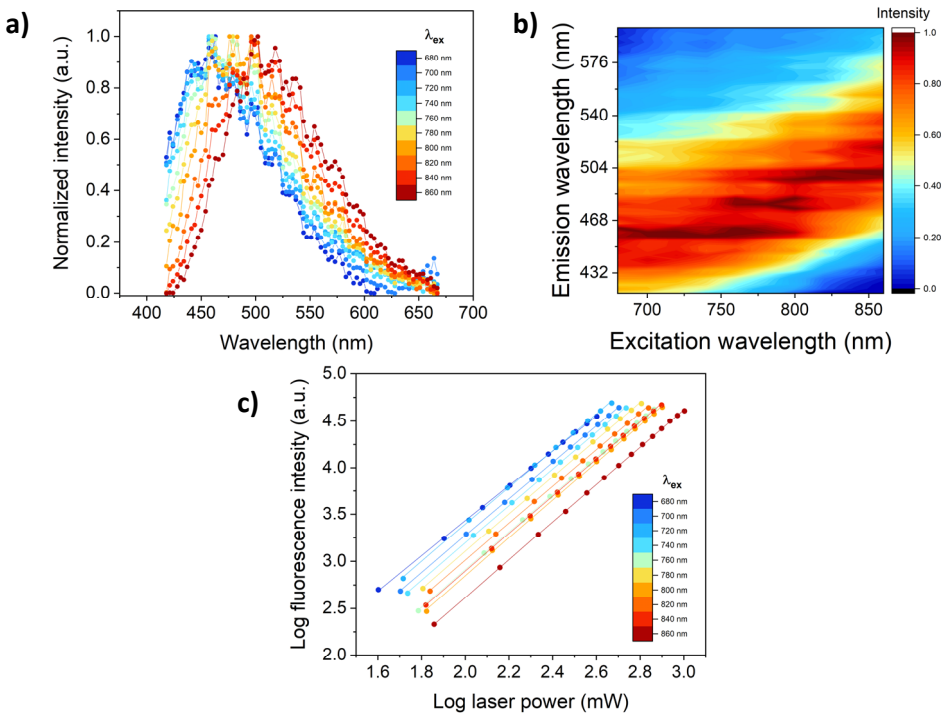

Figure 6.2 (a) UV-Vis emission spectra of the CNQDs (4.0 g/L) under excitation with the fluorescence microscope. **(b)** 3D emission spectra, extracted from (a). **(c)** Log-log plot of emission intensity *vs* excitation power.

In the 3D emission graph in 2PA it is observed that there are three different bands with peaks at 450, 477 and 500 nm (Fig. 6.2-b). This is in contrast to what is observed in the 1PA regime, whose heatmap shows that the emission peak shows a continuous wavelength-dependence between (Fig. 6.1-c). This behavior may indicate that with 2PA it is possible to access different energy levels or different populations depending on the particle size and surface traps in the QDs. Furthermore, the emission resulting from 2PA does not match with that performed with 1PA. For example, with excitation at 760 nm the emission resembles excitation at 410 nm. This behavior has already been reported as 2PA accessing different energy levels in surface traps.[165] However, further investigation must be done with the CNQDs to distinguish the cause of this emission spectra mismatch between 1PA and 2PA and the stepwise emission under 2PA, since this has not been reported previously, likely due to the limited characterization of QDs across such a wide excitation wavelength range.

The 2PA performance of the CNQDs were also evaluated using a femtosecond laser for excitation of a CNQD sample in water in a 1 cm cuvette, (60 fs pulse, repetition frequency 3.0 kHz). Excitation wavelength and power were varied between 700 and 760 nm, and 0.2 to 1.6 mW, respectively. Longpass (600 nm) and neutral density filters and a converging lens were used to control the excitation beam reaching the sample. For excitation powers between 0.2 and 0.8 mW the emission intensity showed a quadratic behavior, while higher excitation power resulted in a pronounced instantaneous increase in emission intensity and a shift to linear dependence on excitation power. This can be explained with white light generation in water. Control

experiments showed that with water only, the same excitation conditions resulted in observation of white light from the cuvette. Thus, at high excitation powers the apparent emission can originate from many different processes including 1PA excitation from the white light.

6.3 Estimation of the Two-Photon Absorption Cross Section

In 1PA, the molar absorptivity represents the probability of a transition to occur. Furthermore, the absorption cross section at 1PA is related to the size of the chromophore and can be described as an effective area in cm^2. For 2PA, the cross section unit is cm^4s/photons, which is generally reported as GM (1 GM = 10^{-50} cm^4s/photons). The meaning remains the effective area of chromophore for photon absorption, however as the number of photons absorbed per second is proportional to the square of the absorption intensity, the cross section cannot have just an area unit.[38, 42, 55] Although there are many works in the literature on carbon-based QDs, few report values for the cross section.[166-169]

Two types of methods are used for experimental determination of 2PA cross section (σ), direct methods (non-linear transmission and Z-scan) and indirect methods. The indirect method is similar to that used to determine the quantum yield (Eq. 2.4), in which the photoluminescence is measured and compared with a reference chromophore, excited under the same 2PA conditions of the sample, whose cross section is known (Eq. 6.1).[170]

$$\sigma = \sigma_{ref} \frac{C_{ref}}{C} \frac{\eta_{ref}}{\eta} \frac{\Phi_{ref}}{\Phi} \frac{F}{F_{ref}} \tag{6.1}$$

where the subscript ref refers to the reference compound, C is the concentration, η is the refractive index of the solvent and F is the integrated emission spectrum. This indirect method was chosen to determine the cross section of the CNQDs studied here due to the ease of performing the experiments. Rhodamine B in air saturated methanol was used as reference (η = 1.3284, Φ = 71%, C = 0.05 μM, σ = 67 – 300 GM between 380 – 860 nm)[171].

Equation 6.1 requires the concentration in molarity, therefore the molecular weight or molar absorptivity of the QDs is necessary for unit conversion. The molar mass was approximated using a simple computational model built upon established CNQD crystal structures found in the Cambridge Structural Database (CSD). The model employed a straightforward carbon nitride structure with a heptazine-base layer pattern featuring dimensions of approximately 1.0 x 1.0 nm. The calculated molecular weight was 2441.9 g/mol with a molecular formula $C_{78}N_{104}H_{48}$. The carboxylate groups introduced into the lattice by addition of EDTA were not included for simplicity.

For particles with a diameter of 6 nm, as determined for the CNQDs in this work, σ = 376 GM at 700 nm. Consideration of larger particle sizes, such as 10 nm, results in an increase cross section of 1741 GM. Although there are numerous works with CNQDs that explore the 2PA process, the determination of the cross section was found in only one. Xie et al. reported σ = 28000 GM for QDs of average size of 4 nm, which is much

higher than the value found here.[166] For carbon QDs the reported σ has values between 31 and 1174 GM, for particle sizes and photoluminescence properties that can be compared to the CNQDs studied here.

6.4 Discussion

The CNQDs prepared here using a microwave synthetic route were photophysically characterized for the 2PA process. The relationship between the emission intensity and the excitation power presents a quadratic behavior. The photoluminescence response with 1PA presents a continuous shift depending on the excitation wavelength, in the 2PA process this behavior is gradual with the appearance of three bands. This may be due to different energy levels being accessed by the 2PA process. It can also be influenced by the size and shape of the particles, and the traps on the surface. The cross section calculated here, with the aid of a computational model for the size and molecular weight of CNQDs, has an upper limit value of 1741 GM for a QD size of 10 nm and excitation at 700 nm.

Caution is needed in experiments aimed at observing 2PA behavior in water as generation of white light cannot be excluded. This phenomenon may be responsible for exciting the QDs rather than the intended excitation from the long wavelength laser. It was observed that there is an excitation power threshold for the white light generation and below this limit the 2PA process could be studied.

The CNQDs prepared here are promising for application in microscopy of biological tissues, since they are water-soluble, photostable, with absorption in the infrared region. Their use in solar light driven catalysis is more uncertain. While they appear to undergo some 2PA already at relatively low excitation powers, it is hard to imagine that near IR-photons will make a large difference to the catalytic performance. Nonetheless, the upconversion process remains an intriguing phenomenon with remarkable potential.

Notably, the cross section value falls within the same order of magnitude as that of many organic molecules whose synthetic route is laborious. A better understanding of the mechanism of 2PA in the CNQDs may help in improving their structure to increase the cross section and potentially unlocking new avenues for catalytic applications.

7 CONCLUDING REMARKS

In this work, different photon up- and down-conversion materials were evaluated with a focus on their future utility in practical devices.

First, low molecular weight gelators, with chromophores covalently attached to the gelator backbone, were evaluated as functional material for TTA-UC and SF, the idea being that the self-assembly properties of the gels may facilitate desired chromophore-chromophore interactions. For TTA-UC the DPA annihilator was covalently *para*-substituted to the OTHO gelator on aromatic rings number 1 and 2, and also on both rings simultaneously. Using PtOEP as a sensitizer it was possible to obtain UC emission in all cases, with ***p1-DPA*** gel being the best, however, high excitation intensities were necessary to make TTA the main deactivation pathway for the triplet excited state. This is possibly the result of the slow triplet energy transfer rate between the sensitizer and the annihilator, which may be caused by the difficulty of the sensitizer in accessing the annihilator in the gel fibers. In addition, the triplet-triplet annihilation step in ***p1-DPA*** may be more efficient because exciton migration appears to be favored in the structure of this gel.

SF was also tested in self-assembled OTHO gels, using the well-studied SF chromophore TIPS-PC covalently linked to the gelator. This study made it possible to evaluate how photophysical properties are influenced by *ortho*-, *meta*-, and *para*-substitution of TIPS-PC in the four aromatic rings of OTHO gelator. Only *meta*- and *para*-substitutions on rings #1 and #2 formed gels. The gel-forming OTHO derivatives, ***m1-PC***, ***m2-PC***, ***p1-PC*** and ***p2-PC***, all show different behavior in transient absorption studies, and it is therefore likely that the gels favor slightly different chromophore-chromophore orientations and distances in the different gels. In ***m1-PC***, the chromophores appear to interact favorably for SF, since the triplet signal is observed right after the excitation pulse.

The studies of SF and TTA-UC OTHO gel suggests that the OTHO gels are viable as materials for photon conversion. We confirmed the hypothesis that it is possible to control the orientation of chromophores in self-assembling OTHO gels. On the other hand, the low efficiency for triplet energy transfer and triplet-triplet annihilation contradicted our hypothesis. A better understanding of how the substitution patterns affect the self-assembly and thus how chromophores will interact with each other, and the environment is needed. Further studies to understand the energy transfer processes in detail as well as energy migration in the gel structure are also needed.

This work also includes experimental development to utilize Vis-to-UV TTA-UC to excite photocatalysts like TiO_2 with visible light. Here, a combination of an Ir(III)-complex and PPO in solution was used for TTA-UC. Despite the low quantum yield of the TTA-UC and the instability of the sensitizer at high excitation power, it was possible to confirm the characteristic absorption of holes in the valence band and electrons in the conduction band of TiO_2 when excited with the UC emission. Furthermore, we could confirm our hypothesis that it would be possible to perform a reaction with the holes formed in the TTA-UC excited TiO_2 film. The results also showed that photoexcitation using low intensity direct excitation leads to the same behavior. While

these results are encouraging, further work is need both to optimize the UC system and the set-up, for using a more stable sensitizer and minimizing the re-absorption of UC emission, adding a back reflector or a waveguide to direct the UC emission towards the semiconductor.

Finally, we studied the 2PA absorption properties of CNQDs. Under the 1PA regime, CNQDs excited in the range 300-550 nm exhibited typical, excitation wavelength dependent, photoluminescence behavior. Using a femtosecond microscope, excitation between 680 and 800 nm, the 2PA properties could be studied. A pure 2PA process was confirmed and results similar to 1PA excitation were observed. However, a detailed analysis revealed that three distinct emission bands could be distinguished. Possibly the 2PA process has access to different populations that may result from particle size, shape, surface defects that generate traps, and more detailed studies to understand this behavior is needed and underway. Given the lack of reliable methods for 2PA cross sections for this type of material, a method to estimate cross sections was developed. Using Rhodamine-B as a reference and computational modeling for the molecular weight of CNQDs, a size dependent σ value could be calculated, 376 GM for particles with an average size of 6 nm and 1741 GM for average size of 10 nm, when 700 nm is used for excitation. The σ value calculated here is of the same order of magnitude as many organic donor-bridge-acceptor molecules for 2PA that are used in microscopy of biological tissues. A more detailed study of the behavior of CNQDs in the 2PA process may indicate design improvements so that the cross section can be increased and whether this process can have any practical implications for the use of CNQDs as catalysts.

To conclude, the two objectives of this work were achieved. First, by evaluating different photoactive materials on their ability to support photon conversion processes and the potential utility for practical applications. Second, by demonstrating how Vis-to-UV TTA-UC can be applied to circumvent spectral mismatch for TiO_2. This work highlights how the structure of the environment influences SF and TTA-UC. Both processes have the potential to increase the efficiency of photovoltaic devices. Also, the results presented here serve as a basis of application to photo-assist reactions on semiconductor surfaces using Vis-to-UV TTA-UC. The photophysical characterization of the water-soluble CNQDs under the 2PA processes indicates their potential to be used in multiphoton fluorescence imaging.

8 ACKNOWLEDGEMENTS

I thank God for placing in my heart this desire to investigate things and for giving me the skills and values necessary for this.

I dedicate this thesis to my mother Irene, who always encouraged my curiosity and was with me on my research adventures since I was little, at a time when we only used books and the Yellow Pages. I am immensely grateful for the patience, support and all the love from my husband Carlos and my son Linus. Also, my sister Daiane, Jefferson and Márcia for your support and prayers.

To my supervisor Maria Abrahamsson, for her patience, guidance and the freedom given to me to work on these projects. And my examiner Bo Albinsson for his teachings.

Special thanks to the reviewers of this thesis: Andrew, Elin, Hanna Härelind.

Thank you for the valuable exchanges of knowledge in group meetings with Axel, Cassandra, Fredrik, Gerard, Gaowa, Hanna, Hassan, Jessica, Liam, Rasmus, Wera. Also, Mark for the synthesis of the OTHO gelators. To my friends Anna W., Lili and Betül for their kindness. And for the collaboration and support of the co-authors of this work. In short, for everyone who is part of this division of the department and makes this a great working environment.

God bless you all!

9 REFERENCES

1. Matthew P. Johnson, Photosynthesis, *Essays in Biochemistry*, **2016**, 60, 255-273.
2. P. Atkins, J. De Paula, R. Friedman, *Quanta, matter, and change: a molecular approach to physical chemistry*, Oxford University Press, USA, **2009**.
3. M. Grätzel, Solar energy conversion by dye-sensitized photovoltaic cells, *Inorganic chemistry*, **2005**, 44, 6841-6851.
4. A. Carrod, V. Gray, K. Börjesson, Recent advances in triplet-triplet annihilation upconversion and singlet fission, towards solar energy applications, *Energy & Environmental Science*, **2022**.
5. L. Buglioni, F. Raymenants, A. Slattery, S. D. Zondag, T. Noël, Technological innovations in photochemistry for organic synthesis: flow chemistry, high-throughput experimentation, scale-up, and photoelectrochemistry, *Chemical Reviews*, **2021**, 122, 2752-2906.
6. D. K. Dogutan, D. G. Nocera, Artificial photosynthesis at efficiencies greatly exceeding that of natural photosynthesis, *Accounts of Chemical Research*, **2019**, 52, 3143-3148.
7. L. O. Björn, *Photobiology: the science of light and life*, Springer, **2015**.
8. S. H. Yun, S. J. Kwok, Light in diagnosis, therapy and surgery, *Nature Biomedical Engineering*, **2017**, 1, 0008.
9. A. Runemark, S. C. Zacharias, H. Sundén, Visible-light-driven stereoselective annulation of alkyl anilines and dibenzoylethylenes via electron donor–acceptor complexes, *The Journal of Organic Chemistry*, **2021**, 86, 1901-1910.
10. D. Devasia, A. Das, V. Mohan, P. K. Jain, Control of chemical reaction pathways by light–matter coupling, *Annual Review of Physical Chemistry*, **2021**, 72, 423-443.
11. M. Sakar, C. C. Nguyen, M. H. Vu, T. O. Do, Materials and mechanisms of photo-assisted chemical reactions under light and dark conditions: can day–night photocatalysis be achieved?, *ChemSusChem*, **2018**, 11, 809-820.
12. Q. Liu, L.-Z. Wu, Recent advances in visible-light-driven organic reactions, *National Science Review*, **2017**, 4, 359-380.
13. A. Fujishima, K. Honda, Electrochemical photolysis of water at a semiconductor electrode, *Nature*, **1972**, 238, 37-38.
14. I. Ganesh, Solar fuels vis-a-vis electricity generation from sunlight: the current state-of-the-art (a review), *Renewable and Sustainable Energy Reviews*, **2015**, 44, 904-932.
15. D. Gust, T. A. Moore, A. L. Moore, Solar fuels via artificial photosynthesis, *Accounts of Chemical Research*, **2009**, 42, 1890-1898.
16. C. Liu, B. C. Colón, M. Ziesack, P. A. Silver, D. G. Nocera, Water splitting–biosynthetic system with CO2 reduction efficiencies exceeding photosynthesis, *Science*, **2016**, 352, 1210-1213.
17. A. S. f. Testing, M. C. G. o. Weathering, Durability, *Standard tables for reference solar spectral irradiances: direct normal and hemispherical on 37° tilted surface*, ASTM International, **2003**.
18. W. Shockley, H. Queisser, Detailed balance limit of efficiency of p–n junction solar cells, in *Renewable Energy*, Routledge, **2018**, pp. Vol2_35-Vol32_54.

19. V. Gray, K. Moth-Poulsen, B. Albinsson, M. Abrahamsson, Towards efficient solid-state triplet–triplet annihilation based photon upconversion: supramolecular, macromolecular and self-assembled systems, *Coordination Chemistry Reviews*, **2018**, 362, 54-71.

20. M. B. Smith, J. Michl, Singlet fission, *Chemical Reviews*, **2010**, 110, 6891-6936.

21. E. Sundin, R. Ringström, F. Johansson, B. l. Küçüköz, A. Ekebergh, V. Gray, B. Albinsson, J. Mårtensson, M. Abrahamsson, Singlet fission and electron injection from the triplet excited state in diphenylisobenzofuran–semiconductor assemblies: effects of solvent polarity and driving force, *The Journal of Physical Chemistry C*, **2020**, 124, 20794-20805.

22. D. Meroni, A. Monguzzi, F. Meinardi, Photon upconversion in multicomponent systems: role of back energy transfer, *The Journal of Chemical Physics*, **2020**, 153.

23. Y. Y. Cheng, B. Fückel, T. Khoury, R. G. Clady, N. Ekins-Daukes, M. J. Crossley, T. W. Schmidt, Entropically driven photochemical upconversion, *The Journal of Physical Chemistry A*, **2011**, 115, 1047-1053.

24. A. Monguzzi, S. M. Borisov, J. Pedrini, I. Klimant, M. Salvalaggio, P. Biagini, F. Melchiorre, C. Lelii, F. Meinardi, Efficient broadband triplet–triplet annihilation-assisted photon upconversion at subsolar irradiance in fully organic systems, *Advanced Functional Materials*, **2015**, 25, 5617-5624.

25. D. F. Barbosa de Mattos, A. Dreos, M. D. Johnstone, A. Runemark, C. Sauvée, V. Gray, K. Moth-Poulsen, H. Sundén, M. Abrahamsson, Covalent incorporation of diphenylanthracene in oxotriphenylhexanoate organogels as a quasi-solid photon upconversion matrix, *The Journal of Chemical Physics*, **2020**, 153.

26. J. De Wild, A. Meijerink, J. Rath, W. Van Sark, R. Schropp, Upconverter solar cells: materials and applications, *Energy & Environmental Science*, **2011**, 4, 4835-4848.

27. S. P. Hill, T. Dilbeck, E. Baduell, K. Hanson, Integrated photon upconversion solar cell via molecular self-assembled bilayers, *ACS Energy Letters*, **2016**, 1, 3-8.

28. J. R. Bolton, *Solar power and fuels*, Elsevier, **2012**.

29. R. Detz, J. Reek, B. Van Der Zwaan, The future of solar fuels: when could they become competitive?, *Energy & Environmental Science*, **2018**, 11, 1653-1669.

30. Y. Ma, X. Wang, Y. Jia, X. Chen, H. Han, C. Li, Titanium dioxide-based nanomaterials for photocatalytic fuel generations, *Chemical Reviews*, **2014**, 114, 9987-10043.

31. S. N. Sanders, T. H. Schloemer, M. K. Gangishetty, D. Anderson, M. Seitz, A. O. Gallegos, R. C. Stokes, D. N. Congreve, Triplet fusion upconversion nanocapsules for volumetric 3D printing, *Nature*, **2022**, 604, 474-478.

32. D. K. Limberg, J.-H. Kang, R. C. Hayward, Triplet–triplet annihilation photopolymerization for high-resolution 3D printing, *Journal of the American Chemical Society*, **2022**, 144, 5226-5232.

33. S. E. Seo, H.-S. Choe, H. Cho, H.-i. Kim, J.-H. Kim, O. S. Kwon, Recent advances in materials for and applications of triplet–triplet annihilation-based upconversion, *Journal of Materials Chemistry C*, **2022**, 10, 4483-4496.

34. M. Barawi, F. Fresno, R. Perez-Ruiz, V. c. A. de la Peña O'Shea, Photoelectrochemical hydrogen evolution driven by visible-to-ultraviolet photon upconversion, *ACS Applied Energy Materials*, **2018**, 2, 207-211.

35. B. D. Ravetz, A. B. Pun, E. M. Churchill, D. N. Congreve, T. Rovis, L. M. Campos, Photoredox catalysis using infrared light via triplet fusion upconversion, *Nature*, **2019**, 565, 343-346.

36. S. H. Askes, N. L. Mora, R. Harkes, R. I. Koning, B. Koster, T. Schmidt, A. Kros, S. Bonnet, Imaging the lipid bilayer of giant unilamellar vesicles using red-to-blue light upconversion, *Chemical Communications*, **2015**, 51, 9137-9140.

37. Q. Liu, M. Xu, T. Yang, B. Tian, X. Zhang, F. Li, Highly photostable near-IR-excitation upconversion nanocapsules based on triplet–triplet annihilation for in vivo bioimaging application, *ACS Applied Materials & Interfaces*, **2018**, 10, 9883-9888.

38. J. R. Lakowicz, *Principles of fluorescence spectroscopy*, Springer, **2006**.

39. M. Adnan, J. J. Baumberg, G. Vijaya Prakash, Linear and nonlinear optical probing of various excitons in 2D inorganic-organic hybrid structures, *Scientific Reports*, **2020**, 10, 2615.

40. P. Theer, B. Kuhn, D. Keusters, W. Denk, Two-photon microscopy and imaging, *Neurobiology*, **2005**, 77, 5.2.

41. M. Auvray, F. Bolze, D. Naud-Martin, M. Poulain, M. Bossuat, G. Clavier, F. Mahuteau-Betzer, On the road toward more efficient biocompatible two-photon excitable fluorophores, *Chemistry–A European Journal*, **2022**, 28, e202104378.

42. P. A. Shaw, E. Forsyth, F. Haseeb, S. Yang, M. Bradley, M. Klausen, Two-photon absorption: an open door to the NIR-II biological window?, *Frontiers in Chemistry*, **2022**, 10, 921354.

43. A. M. Larson, Multiphoton microscopy, *Nature Photonics*, **2011**, 5, 1-1.

44. L. Mistry, L. Le-Quang, G. Masdeu, W. Björkman, H. Härelind, M. Abrahamsson, Selective photocatalytic reduction of CO2-to-CO in water using a polymeric carbon nitride quantum dot/Fe-porphyrin hybrid assembly, *ChemCatChem*, **2022**, 14, e202200897.

45. W. W. Parson, *Modern optical spectroscopy*, Springer, **2007**.

46. P. W. Atkins, J. De Paula, *Atkins' physical chemistry*, Oxford University Press, **2014**.

47. W. T. Silfvast, *Laser fundamentals*, Cambridge university press, **2004**.

48. A. J. Bard, L. R. Faulkner, H. S. White, *Electrochemical methods: fundamentals and applications*, John Wiley & Sons, **2022**.

49. E. J. Chung, L. Leon, C. Rinaldi, *Nanoparticles for biomedical applications: fundamental concepts, biological interactions and clinical applications*, Elsevier, **2019**.

50. D. Bera, L. Qian, T.-K. Tseng, P. H. Holloway, Quantum dots and their multimodal applications: a review, *Materials*, **2010**, 3, 2260-2345.

51. M. A. Cotta, *Journal*, 2020, **3**, 4920-4924.

52. J. M. Hollas, *Modern spectroscopy*, John Wiley & Sons, **2004**.

53. N. J. Turro, *Modern molecular photochemistry*, University Science Books, **1991**.

54. W. M. McClain, Two-photon molecular spectroscopy, *Accounts of Chemical Research*, **1974**, 7, 129-135.

55. M. Pawlicki, H. A. Collins, R. G. Denning, H. L. Anderson, Two-photon absorption and the design of two-photon dyes, *Angewandte Chemie International Edition*, **2009**, 48, 3244-3266.

56. S. J. Chalk, *IUPAC. Compendium of chemical terminology (the gold book)*, Blackwell Scientific Publications, Oxford, 2nd ed. edn., **1997**.

57. V. Gray, P. Xia, Z. Huang, E. Moses, A. Fast, D. A. Fishman, V. I. Vullev, M. Abrahamsson, K. Moth-Poulsen, M. L. Tang, CdS/ZnS core–shell nanocrystal photosensitizers for visible to UV upconversion, *Chemical Science*, **2017**, 8, 5488-5496.

58. M. N. Paddon-Row, Covalently linked systems based on organic components, *Electron Transfer in Chemistry*, **2001**, 178-271.

59. M. Soler, J. K. McCusker, Distinguishing between Dexter and rapid sequential electron transfer in covalently linked donor− acceptor assemblies, *Journal of the American Chemical Society*, **2008**, 130, 4708-4724.

60. J. T. DuBose, P. V. Kamat, Energy versus electron transfer: managing excited-state interactions in perovskite nanocrystal–molecular hybrids: focus review, *Chemical Reviews*, **2022**, 122, 12475-12494.

61. A. Gilbert, J. E. Baggott, *Essentials of molecular photochemistry*, **1991**.

62. D. Dzebo, K. Borjesson, V. Gray, K. Moth-Poulsen, B. Albinsson, Intramolecular triplet–triplet annihilation upconversion in 9, 10-diphenylanthracene oligomers and dendrimers, *The Journal of Physical Chemistry C*, **2016**, 120, 23397-23406.

63. S. M. Bachilo, R. B. Weisman, Determination of triplet quantum yields from triplet− triplet annihilation fluorescence, *The Journal of Physical Chemistry A*, **2000**, 104, 7711-7714.

64. Y. Zhou, F. N. Castellano, T. W. Schmidt, K. Hanson, On the quantum yield of photon upconversion via triplet–triplet annihilation, *ACS Energy Letters*, **2020**, 5, 2322-2326.

65. A. Haefele, J. r. Blumhoff, R. S. Khnayzer, F. N. Castellano, Getting to the (square) root of the problem: how to make noncoherent pumped upconversion linear, *The Journal of Physical Chemistry Letters*, **2012**, 3, 299-303.

66. F. Edhborg, A. Olesund, B. Albinsson, Best practice in determining key photophysical parameters in triplet–triplet annihilation photon upconversion, *Photochemical & Photobiological Sciences*, **2022**, 21, 1143-1158.

67. A. Olesund, J. Johnsson, F. Edhborg, S. Ghasemi, K. Moth-Poulsen, B. Albinsson, Approaching the spin-statistical limit in visible-to-ultraviolet photon upconversion, *Journal of the American Chemical Society*, **2022**, 144, 3706-3716.

68. B. J. Walker, A. J. Musser, D. Beljonne, R. H. Friend, Singlet exciton fission in solution, *Nature Chemistry*, **2013**, 5, 1019-1024.

69. D. Casanova, Theoretical modeling of singlet fission, *Chemical Reviews*, **2018**, 118, 7164-7207.

70. J. C. Johnson, A. J. Nozik, J. Michl, The role of chromophore coupling in singlet fission, *Accounts of Chemical Research*, **2013**, 46, 1290-1299.

71. R. Ringström, F. Edhborg, Z. W. Schroeder, L. Chen, M. J. Ferguson, R. R. Tykwinski, B. Albinsson, Molecular rotational conformation controls the rate of singlet fission and triplet decay in pentacene dimers, *Chemical Science*, **2022**, 13, 4944-4954.

72. T. Ullrich, D. Munz, D. M. Guldi, Unconventional singlet fission materials, *Chemical Society Reviews*, **2021**, 50, 3485-3518.

73. G. L. Closs, J. R. Miller, Intramolecular long-distance electron transfer in organic molecules, *Science*, **1988**, 240, 440-447.

74. M. Gilbert, B. Albinsson, Photoinduced charge and energy transfer in molecular wires, *Chemical Society Reviews*, **2015**, 44, 845-862.

75. M. R. Wasielewski, Photoinduced electron transfer in supramolecular systems for artificial photosynthesis, *Chemical Reviews*, **1992**, 92, 435-461.

76. P. F. Barbara, T. J. Meyer, M. A. Ratner, Contemporary issues in electron transfer research, *The Journal of Physical Chemistry*, **1996**, 100, 13148-13168.

77. J. R. Bolton, M. D. Archer, Basic electron-transfer theory, *Electron Transfer in Inorganic, Organic, and Biological Systems*, **1991**, 228, 7-23.

78. T. Ito, G. J. Meyer, Heme-mediated reduction of organohalide pollutants at nanocrystalline TiO2 thin-film interfaces, *Environmental engineering science*, **2007**, 24, 31-44.

79. S. Lettieri, M. Pavone, A. Fioravanti, L. Santamaria Amato, P. Maddalena, Charge carrier processes and optical properties in TiO2 and TiO2-based heterojunction photocatalysts: a review, *Materials*, **2021**, 14, 1645.

80. M. A. Nadeem, M. A. Khan, A. A. Ziani, H. Idriss, An overview of the photocatalytic water splitting over suspended particles, *Catalysts*, **2021**, 11, 60.

81. G. Bessegato, T. Guaraldo, J. de Brito, M. Brugnera, M. Zanoni, Achievements and trends in photoelectrocatalysis: from environmental to energy applications, in *Electrocatalysis*, Chapter, **2015**, vol. 6, pp. 415-441.

82. H. H. Mohamed, D. W. Bahnemann, The role of electron transfer in photocatalysis: Fact and fictions, *Applied Catalysis B: Environmental*, **2012**, 128, 91-104.

83. E. P. Farr, J. C. Quintana, V. Reynoso, J. D. Ruberry, W. R. Shin, K. R. Swartz, Introduction to time-resolved spectroscopy: nanosecond transient absorption and time-resolved fluorescence of eosin b, *Journal of Chemical Education*, **2018**, 95, 864-871.

84. S. Hoseinkhani, R. Tubino, F. Meinardi, A. Monguzzi, Achieving the photon up-conversion thermodynamic yield upper limit by sensitized triplet–triplet annihilation, *Physical Chemistry Chemical Physics*, **2015**, 17, 4020-4024.

85. V. Gray, A. Dreos, P. Erhart, B. Albinsson, K. Moth-Poulsen, M. Abrahamsson, Loss channels in triplet–triplet annihilation photon upconversion: importance of annihilator singlet and triplet surface shapes, *Physical Chemistry Chemical Physics*, **2017**, 19, 10931-10939.

86. P. Bharmoria, F. Edhborg, H. Bildirir, Y. Sasaki, S. Ghasemi, A. Mårtensson, N. Yanai, N. Kimizuka, B. Albinsson, K. Börjesson, Recyclable optical bioplastics platform for solid state red light harvesting via triplet–triplet annihilation photon upconversion, *Journal of Materials Chemistry A*, **2022**, 10, 21279-21290.

87. X. Yu, X. Cao, X. Chen, N. Ayres, P. Zhang, Triplet–triplet annihilation upconversion from rationally designed polymeric emitters with tunable inter-chromophore distances, *Chemical Communications*, **2015**, 51, 588-591.

88. V. Gray, B. Küçüköz, F. Edhborg, M. Abrahamsson, K. Moth-Poulsen, B. Albinsson, Singlet and triplet energy transfer dynamics in self-assembled axial porphyrin–anthracene complexes: towards supra-molecular structures for photon upconversion, *Physical Chemistry Chemical Physics*, **2018**, 20, 7549-7558.

89. Y. C. Simon, C. Weder, Low-power photon upconversion through triplet–triplet annihilation in polymers, *Journal of Materials Chemistry*, **2012**, 22, 20817-20830.

90. S. H. Lee, J. R. Lott, Y. C. Simon, C. Weder, Melt-processed polymer glasses for low-power upconversion via sensitized triplet–triplet annihilation, *Journal of Materials Chemistry C*, **2013**, 1, 5142-5148.

91. R. Vadrucci, C. Weder, Y. C. Simon, Low-power photon upconversion in organic glasses, *Journal of Materials Chemistry C*, **2014**, 2, 2837-2841.

92. M. Dvořák, S. K. Prasad, C. B. Dover, C. R. Forest, A. Kaleem, R. W. MacQueen, A. J. Petty, R. Forecast, J. E. Beves, J. E. Anthony, Singlet fission in concentrated TIPS-pentacene solutions: the role of excimers and aggregates, *Journal of the American Chemical Society*, **2021**, 143, 13749-13758.

93. C. Grieco, G. S. Doucette, K. T. Munson, J. R. Swartzfager, J. M. Munro, J. E. Anthony, I. Dabo, J. B. Asbury, Vibrational probe of the origin of singlet exciton fission in TIPS-pentacene solutions, *The Journal of Chemical Physics*, **2019**, 151.

94. R. Casillas, I. Papadopoulos, T. Ullrich, D. Thiel, A. Kunzmann, D. M. Guldi, Molecular insights and concepts to engineer singlet fission energy conversion devices, *Energy & Environmental Science*, **2020**, 13, 2741-2804.

95. H. Liu, Z. Wang, X. Wang, L. Shen, C. Zhang, M. Xiao, X. Li, Singlet exciton fission in a linear tetracene tetramer, *Journal of Materials Chemistry C*, **2018**, 6, 3245-3253.

96. N. V. Korovina, N. F. Pompetti, J. C. Johnson, Lessons from intramolecular singlet fission with covalently bound chromophores, *The Journal of Chemical Physics*, **2020**, 152.

97. K. Miyata, F. S. Conrad-Burton, F. L. Geyer, X.-Y. Zhu, Triplet pair states in singlet fission, *Chemical Reviews*, **2019**, 119, 4261-4292.

98. A. Monguzzi, M. Mauri, A. Bianchi, M. K. Dibbanti, R. Simonutti, F. Meinardi, Solid-state sensitized upconversion in polyacrylate elastomers, *The Journal of Physical Chemistry C*, **2016**, 120, 2609-2614.

99. C. Li, C. Koenigsmann, F. Deng, A. Hagstrom, C. A. Schmuttenmaer, J.-H. Kim, Photocurrent enhancement from solid-state triplet–triplet annihilation upconversion of low-intensity, low-energy photons, *ACS Photonics*, **2016**, 3, 784-790.

100. H. Goudarzi, P. E. Keivanidis, All-solution-based aggregation control in solid-state photon upconverting organic model composites, *ACS Applied Materials & Interfaces*, **2017**, 9, 845-857.

101. F. Edhborg, H. Bildirir, P. Bharmoria, K. Moth-Poulsen, B. Albinsson, Intramolecular triplet–triplet annihilation photon upconversion in diffusionally restricted anthracene polymer, *The Journal of Physical Chemistry B*, **2021**, 125, 6255-6263.

102. T. Ogawa, N. Yanai, A. Monguzzi, N. Kimizuka, Highly efficient photon upconversion in self-assembled light-harvesting molecular systems, *Scientific Reports*, **2015**, 5, 10882.

103. S. H. Askes, A. Bahreman, S. Bonnet, Activation of a photodissociative ruthenium complex by triplet–triplet annihilation upconversion in liposomes, *Angewandte Chemie*, **2014**, 126, 1047-1051.

104. A. Turshatov, D. Busko, S. Baluschev, T. Miteva, K. Landfester, Micellar carrier for triplet–triplet annihilation-assisted photon energy upconversion in a water environment, *New Journal of Physics*, **2011**, 13, 083035.

105. Q. Zhou, B. M. Wirtz, T. H. Schloemer, M. C. Burroughs, M. Hu, P. Narayanan, J. Lyu, A. O. Gallegos, C. Layton, D. J. Mai, Spatially controlled UV Light generation at depth using upconversion micelles, *Advanced Materials*, **2022**, 2301563.

106. K. Sripathy, R. W. MacQueen, J. R. Peterson, Y. Y. Cheng, M. Dvořák, D. R. McCamey, N. D. Treat, N. Stingelin, T. W. Schmidt, Highly efficient photochemical upconversion in a quasi-solid organogel, *Journal of Materials Chemistry C*, **2015**, 3, 616-622.

107. R. Vadrucci, C. Weder, Y. C. Simon, Organogels for low-power light upconversion, *Materials Horizons*, **2015**, 2, 120-124.

108. P. Duan, N. Yanai, H. Nagatomi, N. Kimizuka, Photon upconversion in supramolecular gel matrixes: spontaneous accumulation of light-harvesting donor–acceptor arrays in nanofibers and acquired air stability, *Journal of the American Chemical Society*, **2015**, 137, 1887-1894.

109. X. Liu, J. Fei, P. Zhu, J. Li, Facile co-assembly of a dipeptide-based organogel toward efficient triplet–triplet annihilation photonic upconversion, *Chemistry–An Asian Journal*, **2016**, 11, 2700-2704.

110. J. Zhang, Y. Hu, Y. Li, *Gel chemistry: interactions, structures and properties*, Springer, **2018**.

111. Y. Osada, K. Kajiwara, Gels handbook. Volume 1: The fundamentals, *Gels handbook. Volume 1: The fundamentals.*, **2001**.

112. C. Ye, J. Ma, S. Chen, J. Ge, W. Yang, Q. Zheng, X. Wang, Z. Liang, Y. Zhou, Eco-friendly solid-state upconversion hydrogel with thermoresponsive feature as the temperature indicator, *The Journal of Physical Chemistry C*, **2017**, 121, 20158-20164.

113. C. Sauvée, A. Ström, M. Haukka, H. Sundén, A multi-component reaction towards the development of highly modular hydrogelators, *Chemistry–A European Journal*, **2018**, 24, 8071-8075.

114. A. Axelsson, L. Ta, H. Sundén, Direct highly regioselective functionalization of carbohydrates: a three-component reaction combining the dissolving and catalytic efficiency of ionic liquids, *European Journal of Organic Chemistry*, **2016**, 2016, 3339-3343.

115. M. D. Johnstone, C.-W. Hsu, N. Hochbaum, J. Andréasson, H. Sundén, Multi-color emission with orthogonal input triggers from a diarylethene pyrene-OTHO organogelator cocktail, *Chemical Communications*, **2020**, 56, 988-991.

116. L. Ta, A. Axelsson, J. Bijl, M. Haukka, H. Sundén, Ionic liquids as precatalysts in the highly stereoselective conjugate addition of α, β-unsaturated aldehydes to chalcones, *Chemistry–A European Journal*, **2014**, 20, 13889-13893.

117. S. C. Zacharias, M. Kamlar, H. Sundén, Exploring supramolecular gels in flow-type chemistry—Design and preparation of stationary phases, *Industrial & Engineering Chemistry Research*, **2021**, 60, 10056-10063.

118. S.-Y. Hwang, D. Song, E.-J. Seo, F. Hollmann, Y. You, J.-B. Park, Triplet–triplet annihilation-based photon-upconversion to broaden the wavelength spectrum for photobiocatalysis, *Scientific Reports*, **2022**, 12, 9397.

119. O. Vepris, C. Eich, Y. Feng, G. Fuentes, H. Zhang, E. L. Kaijzel, L. J. Cruz, Optically coupled PtOEP and DPA molecules encapsulated into PLGA-nanoparticles for cancer bioimaging, *Biomedicines*, **2022**, 10, 1070.

120. K. M. Felter, F. C. Grozema, Singlet fission in crystalline organic materials: recent insights and future directions, *The Journal of Physical Chemistry Letters*, **2019**, 10, 7208-7214.

121. A. Rao, R. H. Friend, Harnessing singlet exciton fission to break the Shockley–Queisser limit, *Nature Reviews Materials*, **2017**, 2, 1-12.

122. M. W. Wilson, A. Rao, J. Clark, R. S. S. Kumar, D. Brida, G. Cerullo, R. H. Friend, Ultrafast dynamics of exciton fission in polycrystalline pentacene, *Journal of the American Chemical Society*, **2011**, 133, 11830-11833.

123. M. J. Tayebjee, K. N. Schwarz, R. W. MacQueen, M. Dvořák, A. W. Lam, K. P. Ghiggino, D. R. McCamey, T. W. Schmidt, G. J. Conibeer, Morphological evolution and singlet fission in aqueous suspensions of TIPS-pentacene nanoparticles, *The Journal of Physical Chemistry C*, **2016**, 120, 157-165.

124. R. D. Pensack, A. J. Tilley, C. Grieco, G. E. Purdum, E. E. Ostroumov, D. B. Granger, D. G. Oblinsky, J. C. Dean, G. S. Doucette, J. B. Asbury, Striking the right balance of intermolecular coupling for high-efficiency singlet fission, *Chemical Science*, **2018**, 9, 6240-6259.

125. V. Gray, D. Dzebo, A. Lundin, J. Alborzpour, M. Abrahamsson, B. Albinsson, K. Moth-Poulsen, Photophysical characterization of the 9, 10-disubstituted anthracene chromophore and its applications in triplet–triplet annihilation photon upconversion, *Journal of Materials Chemistry C*, **2015**, 3, 11111-11121.

126. A.-K. Bansal, W. Holzer, A. Penzkofer, T. Tsuboi, Absorption and emission spectroscopic characterization of platinum-octaethyl-porphyrin (PtOEP), *Chemical Physics*, **2006**, 330, 118-129.

127. J. Zirzlmeier, R. Casillas, S. R. Reddy, P. B. Coto, D. Lehnherr, E. T. Chernick, I. Papadopoulos, M. Thoss, R. R. Tykwinski, D. M. Guldi, Solution-based intramolecular singlet fission in cross-conjugated pentacene dimers, *Nanoscale*, **2016**, 8, 10113-10123.

128. A. Fujishima, X. Zhang, D. A. Tryk, TiO2 photocatalysis and related surface phenomena, *Surface science reports*, **2008**, 63, 515-582.

129. J. Schneider, M. Matsuoka, M. Takeuchi, J. Zhang, Y. Horiuchi, M. Anpo, D. W. Bahnemann, Understanding TiO2 photocatalysis: mechanisms and materials, *Chemical Reviews*, **2014**, 114, 9919-9986.

130. L. E. Oi, M.-Y. Choo, H. V. Lee, H. C. Ong, S. B. Abd Hamid, J. C. Juan, Recent advances of titanium dioxide (TiO2) for green organic synthesis, *RSC Advances*, **2016**, 6, 108741-108754.

131. Y. Nosaka, Water photo-oxidation over TiO2—history and reaction mechanism, *Catalysts*, **2022**, 12, 1557.

132. R. Giovannetti, C. D. Amato, M. Zannotti, E. Rommozzi, R. Gunnella, M. Minicucci, A. Di Cicco, Visible light photoactivity of polypropylene coated nano-TiO2 for dyes degradation in water, *Scientific Reports*, **2015**, 5, 17801.

133. M. Morsella, N. d'Alessandro, A. E. Lanterna, J. C. Scaiano, Improving the sunscreen properties of TiO2 through an understanding of its catalytic properties, *Acs Omega*, **2016**, 1, 464-469.

134. L. Hou, A. Olesund, S. Thurakkal, X. Zhang, B. Albinsson, Efficient visible-to-UV photon upconversion systems based on CdS nanocrystals modified with triplet energy mediators, *Advanced Functional Materials*, **2021**, 31, 2106198.

135. T. W. Schmidt, F. N. Castellano, Photochemical upconversion: the primacy of kinetics, *The Journal of Physical Chemistry Letters*, **2014**, 5, 4062-4072.

136. N. Harada, Y. Sasaki, M. Hosoyamada, N. Kimizuka, N. Yanai, Discovery of key TIPS-naphthalene for efficient visible-to-UV photon upconversion under sunlight and room light, *Angewandte Chemie International Edition*, **2021**, 60, 142-147.

137. Y. Murakami, A. Motooka, R. Enomoto, K. Niimi, A. Kaiho, N. Kiyoyanagi, Visible-to-ultraviolet (< 340 nm) photon upconversion by triplet–triplet annihilation in solvents, *Physical Chemistry Chemical Physics*, **2020**, 22, 27134-27143.

138. T. Yoshihara, R. Katoh, A. Furube, Y. Tamaki, M. Murai, K. Hara, S. Murata, H. Arakawa, M. Tachiya, Identification of reactive species in photoexcited nanocrystalline TiO2 films by wide-wavelength-range (400− 2500 nm) transient absorption spectroscopy, *The Journal of Physical Chemistry B*, **2004**, 108, 3817-3823.

139. A. Safrany, R. Gao, J. Rabani, Optical properties and reactions of radiation induced TiO2 electrons in aqueous colloid solutions, *The Journal of Physical Chemistry B*, **2000**, 104, 5848-5853.

140. J. Tang, J. R. Durrant, D. R. Klug, Mechanism of photocatalytic water splitting in TiO2. Reaction of water with photoholes, importance of charge carrier dynamics, and evidence for four-hole chemistry, *Journal of the American Chemical Society*, **2008**, 130, 13885-13891.

141. G. Rothenberger, J. Moser, M. Graetzel, N. Serpone, D. K. Sharma, Charge carrier trapping and recombination dynamics in small semiconductor particles, *Journal of the American Chemical Society*, **1985**, 107, 8054-8059.

142. B. Choudhury, A. Choudhury, Local structure modification and phase transformation of TiO2 nanoparticles initiated by oxygen defects, grain size, and annealing temperature, *International Nano Letters*, **2013**, 3, 1-9.

143. S. Pawar, M. Chougule, D. Dalavi, P. Patil, A. Moholkar, S. Sen, J. Kim, V. Patil, Effect of annealing on microstructural and optoelectronic properties of nanocrystalline TiO2 thin films, *Journal of Experimental Nanoscience*, **2013**, 8, 500-508.

144. A. Kafizas, X. Wang, S. R. Pendlebury, P. Barnes, M. Ling, C. Sotelo-Vazquez, R. Quesada-Cabrera, C. Li, I. P. Parkin, J. R. Durrant, Where do photogenerated holes go in anatase: rutile TiO2? A transient absorption spectroscopy study of charge transfer and lifetime, *The Journal of Physical Chemistry A*, **2016**, 120, 715-723.

145. H. H. Mohamed, C. B. Mendive, R. Dillert, D. W. Bahnemann, Kinetic and mechanistic investigations of multielectron transfer reactions induced by stored electrons in TiO2 nanoparticles: a stopped flow study, *The Journal of Physical Chemistry A*, **2011**, 115, 2139-2147.

146. R. S. Khnayzer, J. Blumhoff, J. A. Harrington, A. Haefele, F. Deng, F. N. Castellano, Upconversion-powered photoelectrochemistry, *Chemical Communications*, **2012**, 48, 209-211.

147. Y. Yan, W. Shi, W. Peng, Y. Lin, C. Zhang, L. Li, Y. Sun, H. Ju, J. Zhu, W. Ma, Proton-free electron-trapping feature of titanium dioxide nanoparticles without the characteristic blue color, *Communications Chemistry*, **2019**, 2, 88.

148. G. Boschloo, A. Hagfeldt, Characteristics of the iodide/triiodide redox mediator in dye-sensitized solar cells, *Accounts of Chemical Research*, **2009**, 42, 1819-1826.

149. J. G. Rowley, B. H. Farnum, S. Ardo, G. J. Meyer, Iodide chemistry in dye-sensitized solar cells: making and breaking I− I bonds for solar energy conversion, *The Journal of Physical Chemistry Letters*, **2010**, 1, 3132-3140.

150. B. O'regan, M. Grätzel, A low-cost, high-efficiency solar cell based on dye-sensitized colloidal TiO2 films, *Nature*, **1991**, 353, 737-740.

151. A. Turolla, A. Piazzoli, J. F. Budarz, M. R. Wiesner, M. Antonelli, Experimental measurement and modelling of reactive species generation in TiO2 nanoparticle photocatalysis, *Chemical Engineering Journal*, **2015**, 271, 260-268.

152. F. P. García de Arquer, D. V. Talapin, V. I. Klimov, Y. Arakawa, M. Bayer, E. H. Sargent, Semiconductor quantum dots: technological progress and future challenges, *Science*, **2021**, 373, eaaz8541.

153. D. R. Larson, W. R. Zipfel, R. M. Williams, S. W. Clark, M. P. Bruchez, F. W. Wise, W. W. Webb, Water-soluble quantum dots for multiphoton fluorescence imaging in vivo, *Science*, **2003**, 300, 1434-1436.

154. M. Albota, D. Beljonne, J.-L. Bredas, J. E. Ehrlich, J.-Y. Fu, A. A. Heikal, S. E. Hess, T. Kogej, M. D. Levin, S. R. Marder, Design of organic molecules with large two-photon absorption cross sections, *Science*, **1998**, 281, 1653-1656.

155. H. Dai, X. Gao, E. Liu, Y. Yang, W. Hou, L. Kang, J. Fan, X. Hu, Synthesis and characterization of graphitic carbon nitride sub-microspheres using microwave method under mild condition, *Diamond and Related Materials*, **2013**, 38, 109-117.

156. X. Fan, Y. Feng, Y. Su, L. Zhang, Y. Lv, A green solid-phase method for preparation of carbon nitride quantum dots and their applications in chemiluminescent dopamine sensing, *RSC Advances*, **2015**, 5, 55158-55164.

157. R. Singh, R. Kumar, D. Singh, R. Savu, S. Moshkalev, Progress in microwave-assisted synthesis of quantum dots (graphene/carbon/semiconducting) for bioapplications: a review, *Materials Today Chemistry*, **2019**, 12, 282-314.

158. P. Zhao, B. Jin, Q. Zhang, R. Peng, High-quality carbon nitride quantum dots on photoluminescence: effect of carbon sources, *Langmuir*, **2021**, 37, 1760-1767.

159. Y. Zhan, Z. Liu, Q. Liu, D. Huang, Y. Wei, Y. Hu, X. Lian, C. Hu, A facile and one-pot synthesis of fluorescent graphitic carbon nitride quantum dots for bio-imaging applications, *New Journal of Chemistry*, **2017**, 41, 3930-3938.

160. Y. Wang, J. Wang, P. Ma, H. Yao, L. Zhang, Z. Li, Synthesis of fluorescent polymeric carbon nitride quantum dots in molten salts for security inks, *New Journal of Chemistry*, **2017**, 41, 14918-14923.

161. Z. Zhou, Y. Shen, Y. Li, A. Liu, S. Liu, Y. Zhang, Chemical cleavage of layered carbon nitride with enhanced photoluminescent performances and photoconduction, *ACS Nano*, **2015**, 9, 12480-12487.

162. Y. Tang, Y. Su, N. Yang, L. Zhang, Y. Lv, Carbon nitride quantum dots: a novel chemiluminescence system for selective detection of free chlorine in water, *Analytical Chemistry*, **2014**, 86, 4528-4535.

163. B. S. Haq, H. U. Khan, K. Alam, M. Ajmal, S. Attaullah, I. Zari, Determination of two-photon absorption cross sections of photosensitizers and its implications for two-photon polymerization, *Applied Optics*, **2015**, 54, 132-140.

164. C. Xu, W. W. Webb, Measurement of two-photon excitation cross sections of molecular fluorophores with data from 690 to 1050 nm, *Journal of the Optical Society of America B*, **1996**, 13, 481-491.

165. G. E. LeCroy, F. Messina, A. Sciortino, C. E. Bunker, P. Wang, K. S. Fernando, Y.-P. Sun, Characteristic excitation wavelength dependence of fluorescence emissions in carbon "quantum" dots, *The Journal of Physical Chemistry C*, **2017**, 121, 28180-28186.

166. X. Zhang, H. Wang, H. Wang, Q. Zhang, J. Xie, Y. Tian, J. Wang, Y. Xie, Single-layered graphitic-C3N4 quantum dots for two-photon fluorescence imaging of cellular nucleus, *Advanced Materials*, **2014**, 26, 4438-4443.

167. P. Wang, L. Tian, X. Gao, Y. Xu, P. Yang, Two-photon absorption in a defect-engineered carbon nitride polymer drives red-light photocatalysis, *ChemCatChem*, **2020**, 12, 4185-4197.

168. W. Wang, C. Y. Jimmy, Z. Shen, D. K. Chan, T. Gu, gC3N4 quantum dots: direct synthesis, upconversion properties and photocatalytic application, *Chemical Communications*, **2014**, 50, 10148-10150.

169. Z. Chen, T. Fan, M. Shao, X. Yu, Q. Wu, J. Li, W. Fang, X. Yi, Simultaneously enhanced photon absorption and charge transport on a distorted graphitic carbon nitride toward visible light photocatalytic activity, *Applied Catalysis B: Environmental*, **2019**, 242, 40-50.

170. F. Yuan, Y. Li, X. Li, J. Zhu, L. Fan, S. Zhou, Y. Zhang, J. Zhou, Nitrogen-rich D-π-A structural carbon quantum dots with a bright two-photon fluorescence for deep-tissue imaging, *ACS Applied Bio Materials*, **2018**, 1, 853-858.

171. N. S. Makarov, M. Drobizhev, A. Rebane, Two-photon absorption standards in the 550–1600 nm excitation wavelength range, *Optics Express*, **2008**, 16, 4029-4047.